53 pags

9909

SEMIANNUAL REPORT

TO THE NATIONAL AERONAUTICS AND SPACE ADMINISTRATION

NASA CONTRACT NAG5-459

"Plate Motions and Deformations from Geologic and Geodetic Data"

for the period

1 August 1984 - 31 December 1985

Principal Investigator: Professor Thomas H. Jordan
Department of Earth, Atmospheric, and Planetary Sciences
Massachusetts Institute of Technology
Cambridge, MA 02139

MS 100802

TABLE OF CONTENTS

SIGNIFICANT ACCOMPLISHMENTS

This Semiannual Report covers research conducted under NASA Contract NAG5-459 for the period 1 August 1984 through December 31, 1985.

Our effort on behalf of the Crustal Dynamics Project during that period focused on the development of methodologies suitable for the analysis of space-geodetic data sets for the estimation of crustal motions, in conjunction with results derived from land-based geodetic data, neo-tectonic studies, and other geophysical data. These methodologies were used to provide estimates of both global plate motions and intraplate deformation in the western U.S. Significant accomplishments include:

1. Results from the satellite ranging experiment for the rate of change of the baseline length between San Diego and Quincy, California indicated that relative motion between the North American and Pacific plates over the course of the observing period during 1972-1982 were consistent with esimates calculated from geologic data averaged over the past few million years.

2. This result, when combined with other kinematic constraints on western U.S. deformation derived from land-based geodesy, neo-tectonic studies, and other geophysical data, places limits on the possible extension of the Basin and Range province, and implies significant deformation is occurring west of the San Andreas fault.

3. A new methodology was developed to analyze vector-position space-geodetic data to provide estimates of relative vector motions of the observing sites. The algorithm is suitable for the reduction of large, inhomogeneous data sets, and takes into account the full position covariances, errors due to poorly resolved earth orientation parameters and vertical positions, and reduces baises due to inhomogeneous sampling of the data.

4. This methodology was applied to the problem of estimating the rate-scaling parameter of a global plate tectonic model using satellite laser ranging observations over a five-year interval. The results indicate that the mean rate of global plate motions for that interval are consistent with those averaged over several million years, and are not consistent with quiescent or greatly accelerated plate motions.

5. This methodology was also used to provide constraints on deformation in the western U.S. using very long baseline interferometry observations over a two-year period. Motions

relative to a fixed North American plate frame were consistent with global plate tectonic models at Vandenburg, but were less at Monument Peak, Califonia, suggesting significant deformation west of the San Andreas may be occurring between those sites.

PROBLEMS AND RECOMMENDATIONS

None

DATA UTILITY

Not applicable

FUNDS EXPENDED

As of 31 December 1985, a total of $72,720 had been spent, out of the current fund limitation of $136,500.

APPENDIX I

RELATIVE MOVEMENT OF TECTONIC PLATES IN CALIFORNIA OBSERVED BY SATELLITE LASER RANGING

Abstract: A satellite laser ranging experiment conducted by NASA since 1972 has measured the relative motion between the North America and Pacific plates in California. Based on these measurements, the 896-km distance between San Diego and Quincy, California, is shortening at 62 ± 9 mm/yr. This geodetic estimate is consistent with the rate of motion between the two plates, calculated from geological data to be 53 ± 3 mm/yr, averaged over the past few million years.

Lasers capable of tracking near-earth orbiting satellites have been providing important geodetic data for more than a decade. Beginning in 1972 with the San Andreas Fault Experiment (SAFE), short-term tectonic motions along a baseline spanning the San Andreas system have been monitored by satellite laser ranging (SLR) in an effort to improve our understanding of earthquake hazards in California (Fig. 1). This experiment, which continues as part of NASA's Crustal Dynamics Project, has measured the variations in the 896-km distance between two tracking systems located on opposite sides of the fault with an accuracy unachievable by classical geodetic techniques.

Previous reports (1, 2, 3) have shown the technique to be capable of monitoring short-term (~10 yr) tectonic movements at the centimeter-per-year level. In this paper and the one which follows, we analyze the entire data set collected over the 11-year period 1972-1982 and discuss some of its tectonic implications. In particular, we shall show that space geodetic techniques are beginning to place more stringent constraints on large-scale deformation of the western United States than those derived from classical geological and geophysical observations (4).

Mobile laser systems were used throughout the tracking campaigns. campaigns. Both sites were reoccupied approximately every two years for a duration of several months in order to satisfy certain criteria of data acquisition and, earlier on, tracking geometry. The first results were obtained by tracking a low orbiting spacecraft, Beacon Explorer-C (BE-C), launched in 1965 and equipped with an array of laser retro-reflectors to provide, among other objectives, a spaceborne target for laser engineering studies. In 1976, a dedicated Laser Geodynamics Satellite (LAGEOS) was launched into a high earth orbit with the sole purpose of providing an optimal target for global laser tracking in the context of geodynamic investigations.

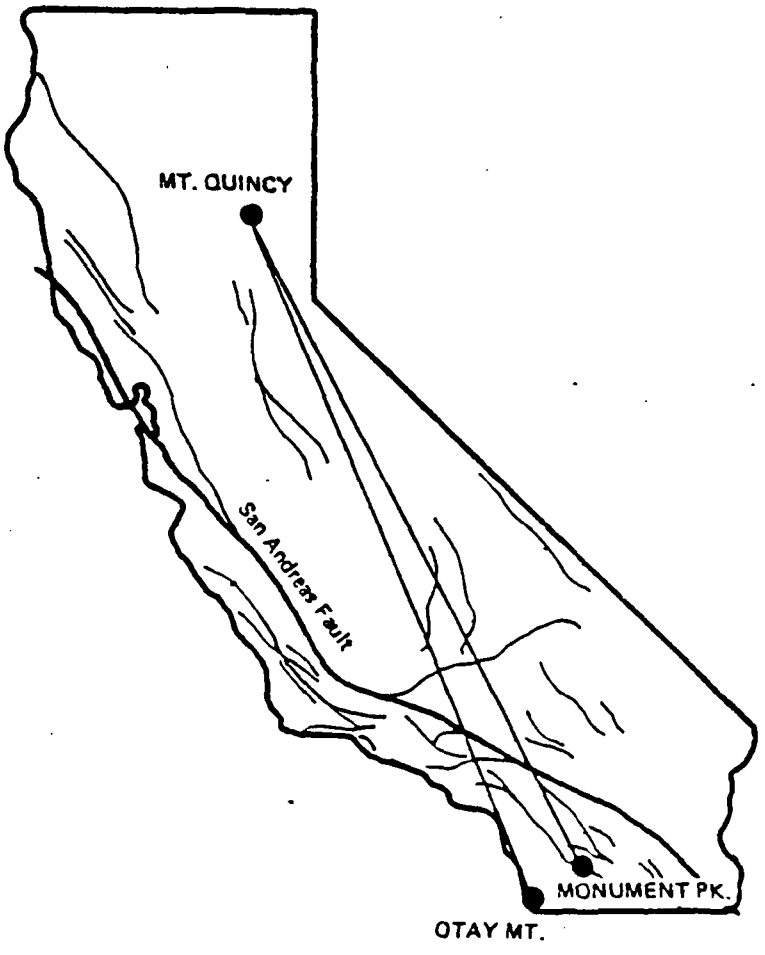

Fig. 1: Map of California showing Quincy-Otay Mt. and Quincy-Monument Pk. baselines measured by satellite laser ranging.

Relative Movement of Tectonic Plates from SLR

In satellite laser ranging, the observed quantities are the nearly instantaneous ranges from a ground station to a spacecraft and the times at which these distances are measured. If the evolution of the orbit and the variations of the earth rotational parameters are known accurately, then the positions of the observing stations (to within an arbitrary shift in absolute longitude) can be calculated in the geocentric reference frame used to describe the satellite motion. Analysis of satellite laser ranging data requires careful consideration of:

(1) the accuracy with which the motion of a near-earth satellite subjected to complex gravitational and non-conservative forces can be modeled,

(2) the accuracy of the observations themselves, which limits the available approaches, and

(3) the requirements of globally distributed tracking support.

BE-C, a low-altitude spacecraft with a complex shape, posed a difficult trajectory modeling problem. Orbital accuracy was severely degraded if more than a few revolutions were analyzed simultaneously; that is, analysis had to be restricted to relatively short arcs. A special data reduction technique was consequently devised to accommodate data collected from two tracking sites only. In spite of its intrinsic limitations for measuring absolute baselines, this technique is capable of detecting changes in the inter-station distance by using uniform tracking geometry and identical force models for each bi-yearly analysis (2, 5).

The launch of LAGEOS at high altitude provided a well-designed laser target far less sensitive to poorly known perturbing forces such as short wavelength gravity and atmospheric drag. With the deployment of a worldwide network of more advanced laser systems, trajectory accuracies achievable for LAGEOS approach the quality of the laser tracking itself, leading to improved estimates of the gravity field at long wavelengths and to highly accurate earth rotational parameters (6, 7). Furthermore, the SAFE line has been incorporated as part of the several hundred lines measured annually in the context of NASA's Crustal Dynamics Project, so that a special data reduction technique is no longer required. Unlike the baselines obtained from BE-C tracking, those derived from LAGEOS are believed to be accurate in an absolute sense (they do, however, depend on the values of $GM_{\oplus}$ and the speed of light used in the reduction procedure).

LAGEOS observations are analyzed in various ways. We have derived robust three-dimensional station positions by combining twelve monthly orbital arcs into annual solutions. In this case, errors arising from weaker data sets and force model imperfections are reduced through averaging over an entire year.

In addition to these annual solutions, we also computed selected subset solutions with finer temporal sampling, which extend the capabilities of SLR to resolve relatively short (<1000 km) baselines, using vastly smaller data sets (from a few

weeks or less). These rely on a short-arc technique, called Baseline Estimation from Simultaneous Tracking (BEST) and involve simultaneous ranging from several sites. Although absolute station positions may be contaminated by unaveraged data and force model errors, these errors cancel in baseline calculations and therefore do not bias the rate-of-change estimates (8).

The use of two different spacecraft results in an inhomogeous set of baseline estimates, which complicates the retrieval of an average rate-of-change for the entire time period covered by the data. Another source of inhomogeneity stems from changes in the locations of ground stations during the experiment. The southern site was changed from Otay Mountain near San Diego, California, to Monument Peak, ~50 km away, in 1981, and the northern site, located near Quincy, California, was moved by about 500 m in 1980. An adequate ground survey tying the two locations with an accuracy comparable to the SLR measurements is available in the latter case, but not in the former. We are therefore dealing with a data set properly described as the juxtaposition of four subsets, each internally homogeneous but having unknown relative offsets in baseline length. These subsets are listed in Table 1, and the individual data points are plotted in Fig. 2. For clarity of graphical presentation, the baseline for each subset is arbitrarily offset by 0.4 m.

We have analyzed the observations presented in Fig. 2 under the assumption that the baseline rate-of-change remained constant for the entire 11-year period covered by the data. The time-dependent baseline length for the ith data subset (i=1,...,4) is therefore given by a modeling equation of the form

$$B_i(t) = \dot{B} \cdot (t-t_0) + B_i^0, \qquad (1)$$

Table 1: SLR data sets used to derive the rate-of-change of the Quincy-San Diego baseline.

Set No.	Satellite	Baseline	Solution Type	No. Pts.	r.m.s. (mm)†	Cumulative Importance
1	BE-C	Quincy-Otay Mt.	Special	4	89	0.26
2	LAGEOS	Quincy-Otay Mt.	Annual	3	37	0.58
3	LAGEOS	Quincy-Mon. Pk.	Annual	2	<1	0.06
4	LAGEOS	Quincy-Mon. Pk.	BEST	14	43	0.10

† Misfit with respect to constant-rate solution of Fig. 2.

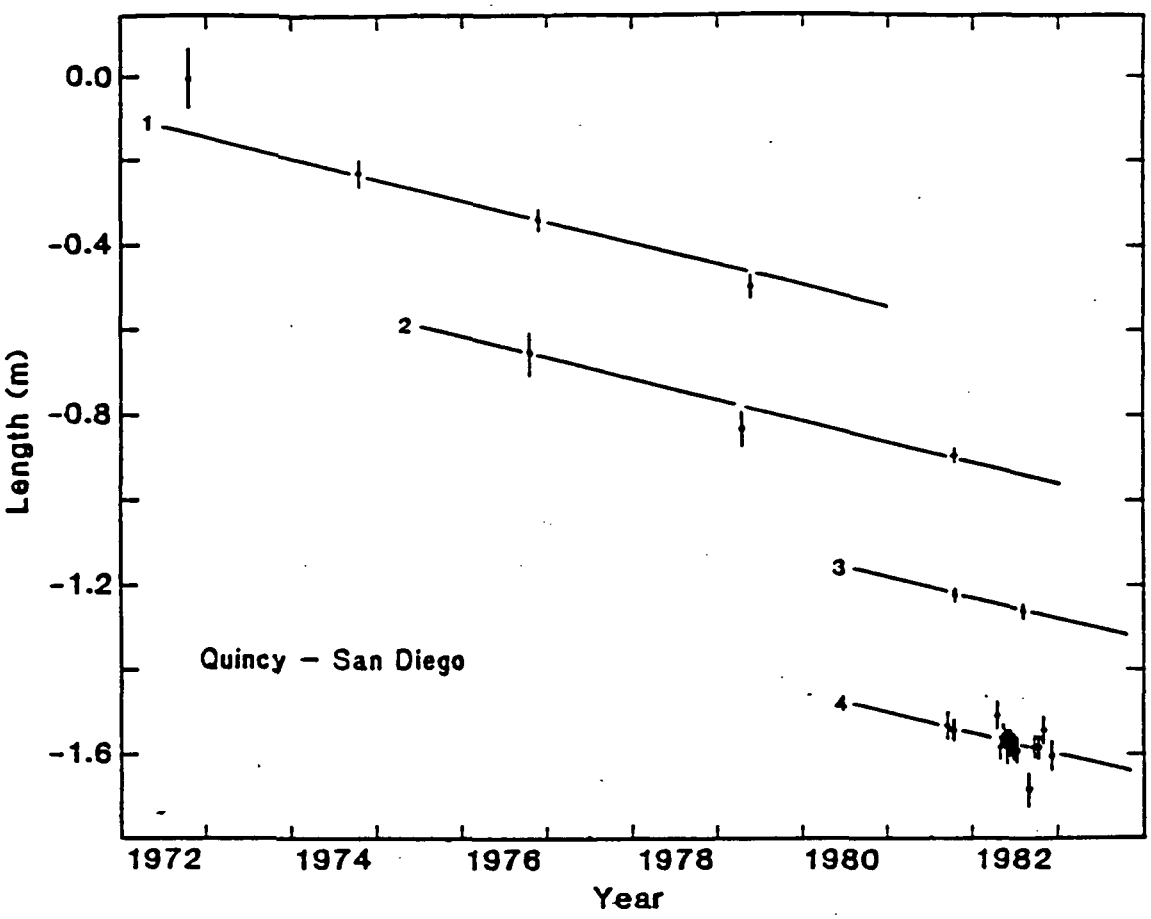

Fig. 2: Variations in the Quincy-San Diego baseline length from SLR measurements between 1972 and 1982. Constant-rate solution was fitted simultaneously to the four data subsets listed in Table 1 and shown here with arbitrary 0.4 m offsets. Error bars are standard deviations obtained from individual baseline estimates.

---

where the intercept B_i^o is the absolute baseline length at the fiducial time t_o, and $\dot{B}$ is a constant rate-of-change.

Because of the offsets in the observed baseline lengths, the B_i^o's as well as $\dot{B}$ must be considered a priori unknown; hence, the data generate a system of 23 equations in 5 unknowns. The four intercepts are only of ancillary interest, so it is not necessary to solve for their values directly. We therefore applied an appropriate projection operator to the linear system to annihilate the dependence of the data on these parameters and then solved for $\dot{B}$ by least-squares. The weights used in the least-squares criterion were chosen to be proportional to the

standard errors depicted on Fig. 2. These formal errors of estimation are appropriate as relative weights within each homogeneous data subset, but there remains a subjective choice regarding the weighting of different subsets with respect to each other. In view of the earlier discussion, we down-weighted the BE-C data relative to the LAGEOS data by a factor of two in order to reflect the greater reliability of the latter. This has the practical effect of nearly equalizing the weights of the most reliable BE-C points and the least reliable LAGEOS points in the inversion.

The least-squares formulation permits calculation of "data importances", additive quantities which represent the information contributed by each datum or data subset to the solution (9). In the present case, since we are estimating the single scalar quantity $\dot{B}$, the data importances of the projected system sum to unity. The cumulative data importances for the four data subsets are listed in Table 1.

The rate-of-change estimate obtained by the least-squares procedure is

$$\dot{B} = -61.7 \pm 8.7 \text{ mm/yr}, \tag{2}$$

where the uncertainty is the standard error of estimation. The r.m.s. residual for this solution is 52 mm, and the weighted r.m.s. residual is 29 mm. As seen on Fig. 2, this solution satisfies all but five observations at the one-sigma level, and all but one of the BEST estimates at the two-sigma level.

The misfit to the 1972 BE-C measurement is no cause for concern, since it was the first collected for the SAFE baseline and is the most uncertain. Its individual importance is only 0.04; that is, it contributes but a small fraction of the information used to estimate $\dot{B}$. In fact, completely removing this first point from the data set merely changes the answer to -59.9 ± 8.9 mm/yr, which is not resolvable from the value quoted above.

The absolute baseline lengths retrieved from the BE-C data and the LAGEOS data for Quincy-Otay (subsets 1 and 2 of Table 1) differ by 0.76 m. While such a discrepancy was not unexpected in view of the differences in data reduction techniques, its size indicates BE-C force-model errors that were somewhat larger than anticipated. However, our claim that the rate is not contaminated by the bias in absolute baseline length is supported by the consistency of the baseline changes between 1976 and 1979 for both spacecraft.

As for the poorly fitted BEST points, it must be noted that this data reduction technique, while minimizing the effects of dynamic errors on the baseline estimate, is quite susceptible to intermittent anomalies which occasionally occur in the laser data. Its reliance on a limited set of strictly simultaneous observations (in reality, manufactured laser "normal points" at two minute intervals) allows little averaging of the errors arising from anomalous data, causing an occasional spurious

baseline estimate. Fortunately, including the three outliers evident in Fig. 2 does not affect the slope estimate derived from the BEST subset. This subset comprises the majority of the data points but does not dominate the estimation of $\dot{B}$; in fact, owing to its short time span, its cumulative data importance is only 0.10.

By far the most important group of observations is the set of three annual LAGEOS solutions for the Quincy-Otay baseline between 1976 and 1982 (subset 2); its cumulative importance is nearly 0.6. These data cover approximately 5 years of observations, so they provide a good constraint on the slope. Subset 2 alone yields a rate of -53.6 $\pm$ 11.4 mm/yr, again not significantly different from Eq. 2.

Tapley et al. (7) produced an independent set of eleven estimates for the Quincy-Monument Pk. baseline from bimonthly arcs between October, 1981 and November, 1983. For this two year period, they deduce a rate-of-change of -64 $\pm$ 9 mm/yr. Their data reduction technique is different from ours, and they extend the coverage by a full year beyond the BEST solutions shown on Fig. 2. It is encouraging, therefore, that their value is in good agreement with Eq. 2.

Assuming the Quincy site lies on a rigid North America plate (NOAM) and the Otay Mt./Monument Pk. sites on a rigid Pacific plate (PCFC), we can compute the baseline rate-of-change using the PCFC-NOAM instantaneous angular velocity vector derived from plate-tectonic data. The eleven-plate model RM2, which satisfies a globally distributed set of marine magnetic rates, transform-fault directions and slip-vector azimuths (10), yields $\dot{B}$ = -52.9 $\pm$ 2.7 mm/yr, consistent at the one-sigma level with the SLR estimate of Eq. 2. This removes the discrepancy noted by Smith et al. (2), who derived a preliminary SLR rate of -90 $\pm$ 30 mm/yr from the 1972-1977 BE-C observations. As shown in Fig. 2, the BE-C and LAGEOS points prior to 1979, taken alone, do indeed suggest a higher value, which could indicate some temporal variation in the apparent rate, but the hypothesis that the deviations from a constant-rate model are random statistical fluctuations cannot be rejected at even a low confidence level (11).

Demosthenes C. CHRISTODOULIDIS
David E. SMITH

Geodynamics Branch, Goddard Space Flight Center,
Greenbelt, Maryland 20771

J. Bernard MINSTER

Science Horizons, Inc., 710 Encinitas Blvd.,
Encinitas, California 92024

Thomas H. JORDAN

Dept. of Earth, Atmospheric and Planetary Sciences,

Massachusetts Institute of Technology,
Cambridge, Massachusetts 02139

References and Notes

(1) D. E. Smith, R. Kolenkiewicz, G. H. Wyatt, P. J. Dunn, M. H. Torrence, Phil. Trans. R. Soc. London, A 284, 529-536 (1977).

(2) D. E. Smith, R. Kolenkiewicz, P. J. Dunn, M. H. Torrence, Tectonophysics 52, 59-67 (1979).

(3) D. E. Smith, NASA TM 80642, 3.40-3.42 (1980); D. C. Christodoulidis and D. E. Smith, NASA TM 86123, 1.2-1.5 (1984).

(4) J. B. Minster and T. H. Jordan, in **Tectonics and Sedimentation along the California Margin**, J. K. Crouch and S. B. Bachman, Eds. (Pacific Sect. Soc. Econ. Paleontol. Mineral. 38, 1984), pp. 1-16.

(5) R. W. Agreen and D. E. Smith, J. Geophys. Res. 79, 4413-4417 (1974).

(6) F. J. Lerch, S. M. Klosko, G. B. Patel, Geophys. Res. Lett. 9, 1263-1266 (1982); W. E. Carter, D. S. Robertson, J. E. Pettey, B. D. Tapley, B. E. Schutz, R. J. Eanes, Science 224, 957-961 (1984).

(7) B. D. Tapley, B. E. Schutz, R. J. Eanes, J. Geophys. Res. 89, in press (1984).

(8) D. C. Christodoulidis and D. E. Smith, NASA TM 82133 (1982); D. C. Christodoulidis, D. E. Smith, R. Kolenkiewicz, S. M. Klosko, M. H. Torrence, P. J. Dunn, J. Geophys. Res. 89, in press (1984).

(9) J. B. Minster, T. H. Jordan, P. Molnar, E. Haines, Geophys. J. R. astr. Soc. 36, 541-576 (1974).

(10) J. B. Minster and T. H. Jordan, J. Geophys. Res. 83, 5331-5354 (1978).

(11) In a Wald-Wolfowitz run test on the distribution of normalized residuals above and below the median, the observed number of runs is 10; under the null hypothesis that this sequence is random, the expected number is 12.0 with a variance of 5.3.

(12) This research was supported by the National Aeronautics and Space Administration, under NASA's Crustal Dynamics Project. We are grateful to P. J. Dunn, S. M. Klosko, R. Kolenkiewicz and M. H. Torrence for their invaluable assistance in the completion of this work.

CONSTRAINTS ON WESTERN U.S. DEFORMATION FROM SATELLITE LASER RANGING

Abstract: The rate of shortening between San Diego and Quincy, California, measured by satellite laser ranging (SLR) is substantially greater than that implied by the rate of slip measured on the San Andreas fault. When combined with other kinematical constraints on western U.S. deformation, these comparisons limit the extension rate across the Great Basin to be less than 9 mm/yr and imply significant deformation of the Pacific plate west of the San Andreas. Along the central California margin, the integrated rate of deformation is estimated to be 18 ± 5 mm/yr and entails compression perpendicular to the San Andreas, as well as right-lateral strike-slip motion parallel to it. Within the framework of our tectonic model, the SLR data limit the integrated deformation rate across the Southern California Borderlands to be less than 7 mm/yr.

The rate-of-change of the Quincy-San Diego baseline (Fig. 1) measured in NASA's San Andreas Fault Experiment (SAFE) since 1972, and more recently by NASA's Crustal Dynamics Project is (1)

$$\dot{B} = -61.7 \pm 8.7 \text{ mm/yr}, \tag{1}$$

The value calculated from the plate-tectonic model RM2 (2) is -52.9 ± 2.7 mm/yr, which assumes Quincy lies on a rigid North America plate (NOAM) and San Diego on a rigid Pacific plate (PCFC). The geodetic estimate of the SAFE baseline shortening rate observed over an eleven-year period is thus compatible with plate motions averaged over a much longer interval (1-3 million years in the case of RM2). However, neither is easily reconciled with the hypothesis that PCFC-NOAM relative motion is localized on the San Andreas fault. We consider two fiducial points juxtaposed on either side of the fault zone, r_C^W just to the west of the San Andreas and r_C^e just to the east, and let v_{SA} be the (steady-state) velocity vector of the former with respect to the latter. In central California, where the fault best approximates a simple transform, a range of geological and geodetic observations local to the fault zone provides the estimate (3, 4)

$$v_{SA} = \begin{cases} 34 \pm 3 \text{ mm/yr} \\ \text{N41°W} \pm 2° \end{cases} \tag{2}$$

The RM2 PCFC-NOAM velocity vector calculated at the fiducial location r_C = 36°N, 120.6°W (Fig. 1) is

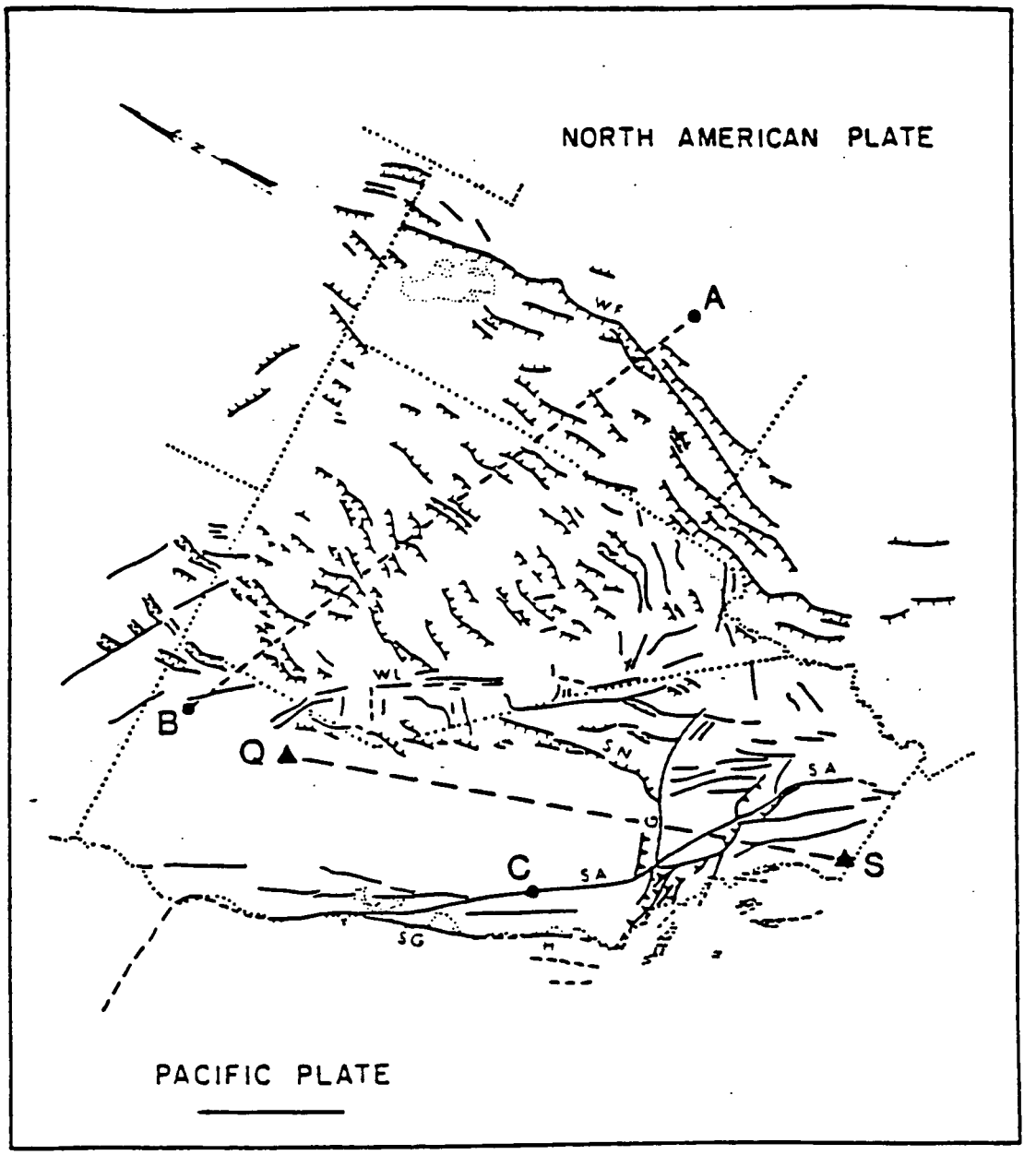

Fig. 1: Oblique Mercator projection of the western United States about the RM2 PCFC-NOAM pole of rotation, showing major Quaternary faults and reference points used in our vector calculations. C is the fiducial point on the San Andreas fault where the vectors in Eqs. 2-6 are specified. AB is the line along which the expansion rate of the Great Basin is defined. Triangles are SLR stations at Quincy (Q) and San Diego (S), California. Faults are from (5) and (6); lettered features are the Garlock fault (G), Hosgri fault (H), San Andreas fault (SA), San Gregorio fault (SG), Sierra Nevada front (SN), Wasatch front (WF), and Walker Lane (WL).

$$v_{PN} = \begin{cases} 55.9 \pm 2.7 \text{ mm/yr} \\ \text{N35.5°W} \pm 1.9° \end{cases} \quad (3)$$

The discrepancy between Eqs. 2 and 3 is significant at the two-sigma level in both rate and azimuth; it is thought to be a measure of the present-day tectonic deformation integrated across a broad zone of PCFC-NOAM interaction that extends from the continental margin of California to the Rocky Mountains (2, 5).

How the deformation represented by this discrepancy is partitioned east and west of the San Andreas is a question of considerable geological interest and seismogenic implications. If v_{CN} is the velocity of the fiducial point r_C^e in the reference frame rotating with NOAM and v_{CP} is the velocity of r_C^w in the PCFC frame, then the discrepancy vector $v_{PN} - v_{SA}$, by definition, must equal $v_{CN} - v_{CP}$: the deformation distributed over a plate boundary zone must sum up to the relative plate velocity. v_{CN} thus summarizes the deformation occurring on the NOAM side of the San Andreas, whereas v_{CP} summarizes the deformation on the PCFC side. We have formulated these vectors in terms of frame-independent integrals of the velocity gradient tensor along paths across the zone of deformation (3).

The distribution of Quaternary faulting shown in Fig. 1, as well as the observed seismicity, defines an essentially rigid Sierra Nevada-Great Valley block (SNGV) extending from the San Andreas eastward to the Sierra Nevada front (5). The relative motion between this block and NOAM is taken up primarily by deformation in the Great Basin of Nevada and western Utah. Stress and strain orientation data pertaining to Quaternary deformation of the Great Basin constrain the direction of this motion to be approximately N60°W (7). These constraints have been used to construct a one-parameter family of kinematical models parameterized by the total rate of expansion across the Great Basin from south-central Utah to northern California (along the line AB in Fig. 1)(3). We define a normalized velocity vector $\hat{v}_{CN}$ by the equation

$$v_{CN}(\alpha) = \alpha \, \hat{v}_{CN}, \quad (4)$$

where α is a dimensionless parameter such that $\alpha \times 10$ mm/yr is the opening rate for this path. In other words, $\hat{v}_{CN}$ is the unique velocity which would describe the local SNGV-NOAM motion at r_C if the Great Basin were expanding at a total rate of exactly 10 mm/yr along AB. As documented in (3), the data compiled by Zoback and Zoback (7) yield the conditional estimate

$$\hat{v}_{CN} = \begin{cases} 10.1 \pm 0.7 \text{ mm/yr} \\ \text{N63°W} \pm 5° \end{cases} \tag{5}$$

The estimation procedure, which is based on a numerical search over possible SNGV-NOAM pole positions, explicitly accounts for sphericity of the earth's surface (on a flat earth, the modulus of $\hat{v}_{CN}$ would be exactly 10 mm/yr).

The locus of v_{CN} parameterized by α is compared with the discrepancy vector $v_{PN} - v_{SA}$ in the upper vector diagram of Fig. 2. Clearly, the opening of the Basin and Range is not in the right direction to account entirely for the discrepancy, regardless of the value of α. This implies that some deformation must be occurring west of the San Andreas fault.

Given the definitions embodied in Eq. 4 and the constraints imposed by the plate-tectonic boundary conditions, the vector summarizing deformation west of the San Andreas can be recast in the form

$$v_{CP}(\alpha) = \alpha \hat{v}_{CN} - (v_{PN} - v_{SA}), \tag{6}$$

and an estimate of v_{CP} conditional on α can be derived from Eqs. 2, 3 and 5. This expression and the corresponding equation for the variance matrix of $v_{CP}(\alpha)$ yield the lower vector diagram in Fig. 2. The locus of $v_{CP}(\alpha)$ is a straight line in the direction of $\hat{v}_{CN}$, and its two-sigma error ellipse sweeps a band approximately 12 mm/yr wide, broadening slightly with increasing α. For values of α near zero, $v_{CP}(\alpha)$ is subparallel to the San Andreas and could be accommodated by predominantly right-lateral faulting localized along, say, the San Gregorio-Hosgri fault system, which parallels the California coastline (Fig. 2). On the other hand, if the Great Basin extension rate were as great as 20 mm/yr ($\alpha = 2$), as some students of Basin-and-Range deformation have advocated (9), then v_{CP} would be essentially perpendicular to the San Andreas and would imply compression across the California margin with very little strike-slip motion. Interpretations of recently published seismic reflection profiles traversing the southern part of the Hosgri fault favor this model (10).

The SLR observations discussed in (1) provide an upper bound on α that excludes this latter possibility. Assuming the Quincy site lies on SNGV and the San Diego sites (Otay Mt. and Monument Pk.) on PCFC, we can derive an estimate of $\dot{B}$ conditional on α by the same procedure used to obtain Eq. 5. The result is

$$\dot{B} = -(52.9 - 7.9\alpha) \pm (7.29 + 0.49\alpha^2)^{\frac{1}{2}} \text{ mm/yr}. \tag{7}$$

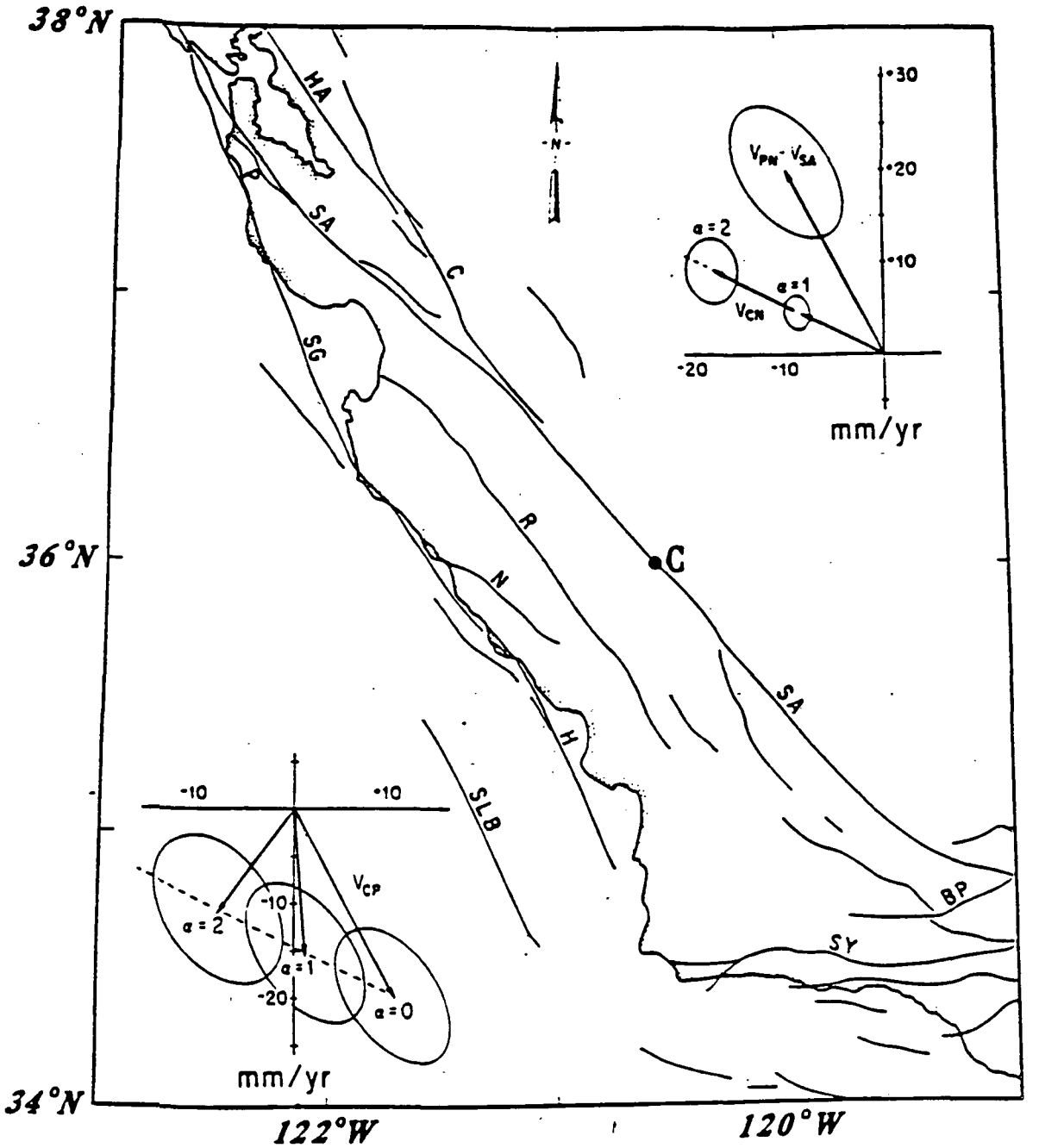

Fig. 2: Map: Lambert conformal conic projection of central California showing major zones of Quaternary faulting (8). Lettered fault zones are the Big Pine (BP), Calaveras (C), Hosgri (H), Nacimiento (N), Pilarcitos (P), Rinconada (R), San Andreas (SA), San Gregorio (SG), Santa Lucia Bank (SLB), and Santa Ynez (SY). C is the fiducial point at 36°N on the San Andreas used in vector calculations. **Upper inset:** Velocity diagram in the tangent plane at C showing discrepancy vector $\mathbf{v}_{PN} - \mathbf{v}_{SA}$ and vector $\mathbf{v}_{CN}(\alpha)$ describing Basin-and-Range deformation; $\alpha = 1$ corresponds to an opening rate of exactly 10 mm/yr across the Great Basin along line AB in Fig. 1. Error ellipses are two-sigma. **Lower inset:** Velocity diagram at C showing $\mathbf{v}_{CP}$, which describes deformation west of the San Andreas. Dashed line is locus parameterized by α. Error ellipses are two-sigma.

As α increases from zero, the total expansion of the Great Basin accelerates, and the agreement between Eqs. 1 and 7 degrades. If α were as great as two, for example, then the value of the SAFE baseline rate-of-change would be -37.1 $\pm$ 3.1 mm/yr, which is not consistent with the SLR results.

A formal upper bound on α can be obtained from Eqs. 1 and 7 by applying a one-sided chi-square test; at the 95% confidence level, we find $\alpha < 0.80$. If instead of Eq. 2 we use the estimate of -64 $\pm$ 9 mm/yr given by Tapley et al. (11), this bound is reduced to 0.56. The chi-square test assumes the standard deviations assigned a priori to the SLR data are exact; scaling these uncertainties to the root-mean-square misfit provided by the constant-slope solution reduces the standard error of $\dot{B}$ in Eq. 1 to 8.3 mm/yr, and applying the appropriate one-sided F test gives $\alpha < 0.89$.

The SLR measurements thus limit the extension rate of the Great Basin to be less than 9 mm/yr. This is consistent with, but more stringent than, the upper bounds obtained from direct geological and geophysical observations of Basin-and-Range deformation (12). Moreover, through Eq. 7, the SLR data constrain the vector v_{CP} to have a significant projection parallel to the San Andreas; the lower bound on this component of motion is 5 mm/yr, and it is likely to be considerably larger (Fig. 2). In fact, our results are consistent with strike-slip rates of 6-17 mm/yr inferred from post-Pliocene offsets along the San Gregorio-Hosgri fault system (13). Hence, a model with purely compressive deformation along the California margin is excluded. We note, however, that α is constrained by observations in the Great Basin to be greater than 0.1 (12), requiring the component of v_{CP} perpendicular to the San Andreas to be greater than zero, as implied by geological observations of regional compression west of the fault (10).

We infer that the rate of deformation west of the San Andreas is large. For $\alpha = 0.9$, our best estimate of v_{CP} has a magnitude of 16 mm/yr, and it is increases to 21 mm/yr for $\alpha = 0.1$. These estimates are one measure of the seismogenic potential of the central California margin.

We have assumed throughout this analysis that the San Diego sites are rigidly attached to PCFC. Any geologically plausible deformation west of these sites -- accommodated, say, on offshore faults within the seismically active California Borderlands-- would imply a decrease in the magnitude of $\hat{B}$ relative to Eq. 7 and, hence, would lower our upper bound on α. For example, the block-tectonic model of southern California developed by Bird and Rosenstock (14) predicts that the San Diego sites move with respect to PCFC at ~3 mm/yr in the direction ~N40°W; such a motion would lower our bound on α from 0.9 to about 0.6. Conversely, a lower bound on α can be used to place an upper bound on the rate at which the San Diego sites translate with respect to PCFC. Assuming this motion is N40°W, and adopting $\alpha > 0.1$, we find that this rate must be less than 7 mm/yr to be

consistent with the SLR data. The integrated rate of deformation across the Southern California Borderlands is therefore inferred to be less than that across the central California margin. Presumably, the difference between these deformation vectors is taken up by the northward compression of the western Tranverse Ranges (14).

The preliminary results in this report point the way to future applications of SLR and other space-geodetic techniques in the study of regional deformation. In particular, they illustrate the advantages of combining SLR measurements with other geological, geophysical and geodetic data sets. When considered in the context of regional kinematical models constructed from such data sets, the SLR observations from a single California baseline yield quantitative constraints on the distribution of deformation in the western United States. Much more stringent constraints can be expected from the large set of North America baselines currently being measured under the auspices of NASA's Crustal Dynamics Project (15). Space-geodetic observations should be especially useful in fixing the rates of regional deformation that are difficult to measure with conventional techniques but are critical to the assessment of seismogenic potential.

Thomas H. JORDAN

Dept. of Earth, Atmospheric and Planetary Sciences,
Massachusetts Institute of Technology,
Cambridge, Massachusetts 02139

J. Bernard MINSTER

Science Horizons, Inc., 710 Encinitas Blvd.,
Encinitas, California 92024

Demosthenes C. CHRISTODOULIDIS
David E. SMITH

Geodynamics Branch, Goddard Space Flight Center,
Greenbelt, Maryland 20771

References and Notes

(1) D. C. Christodoulidis, D. E. Smith, J. B. Minster, T. H. Jordan, Science, this issue (1984).

(2) J. B. Minster and T. H. Jordan, J. Geophys. Res. 83, 5331-5354 (1978).

(3) J. B. Minster and T. H. Jordan, in **Tectonics and Sedimentation along the California Margin**, J. K. Crouch and S. B. Bachman, Eds. (Pacific Sect. Soc. Econ. Paleontol. Mineral. 38, 1984), pp. 1-16.

(4) K. E. Sieh and R. H. Jahns, Geol. Soc. Amer. Bull. 95, 883-896 (1984).

(5) D. P. Hill, J. Geophys. Res. 87, 5433-5450 (1982).

(6) L. Wright, Geology 4, 489-494 (1976).

(7) M. L. Zoback and M. D. Zoback, J. Geophys. Res. 85, 275-284 (1980); M. L. Zoback and M. D. Zoback, J. Geophys. Res. 85, 6113-6156 (1980).

(8) C. W. Jennings, Calif. Geol. Data Map Ser., map 1, Calif. Div. of Mines and Geol., Sacramento (1975); San Gregorio-Hosgri Fault Zone, California, E. A. Silver and W. R. Normark, Eds. (Calif. Div. of Mines and Geol. Spec. Rep. 137, 1978), pp. 1-56.

(9) Thompson and Burke (16) showed that Dixie Valley has widened in a N55°W direction at an average rate of ~1 mm/yr over the past 12,000 years. Assuming uniform strain and extrapolating this result to the entire province, they infer a total Basin-and-Range expansion rate of ~20 mm/yr. Integration of the strain rate estimates of Greensfelder et al. (17) along line AB of Fig. 1 yields a total rate in excess of 40 mm/yr, although their tabulated seismic moment rates for historic seismicity are consistent with 5-22 mm/yr (4).

(10) Crouch et al. (18) argued that offshore seismic reflection profiles near 35°N indicate a dominance of reverse faulting, and that the parallelism of fold axes and fault strikes is inconsistent with large scale right-lateral motion. Compression west of the San Andreas is also supported by geodetic and geological evidence (19), and by the distribution of compressive axes for earthquake fault-plane solutions (20).

(11) B. D. Tapley, B. E. Schutz, R. J. Eanes, J. Geophys. Res. 89, in press (1984).

(12) Late Cenozoic (10-17 Myr) estimates of the Great Basin expansion rate range from 3 to 20 mm/yr (3, 21). Rates more appropriate for the study of Quaternary deformation can be derived from Holocene paleoseismic mapping; Wallace's (22) data yield 1-12 mm/yr along the line AB of Fig. 1 (3). The lower bound, which corresponds to $\alpha \geq 0.1$, is set by Thompson and Burke's (16) rate for Dixie Valley.

(13) About 100 km of right-lateral displacement on the San Gregorio-Hosgri fault system has been suggested (23). By modeling the Santa Maria Basin as a pull-apart structure, Hall (24) obtained a "generalized estimate" of 30-50 km over the past 3 Myr, for an average rate of 10-17 mm/yr across the Hosgri fault. Based on offsets of marine terraces over the last 200,000 years at Pt. Año Nuevo, California, Weber and Lajoie (25) argued for a rate of 6-13 mm/yr across the San Gregorio fault.

(14) P. Bird and R. W. Rosenstock, Geol. Soc. Amer. Bull. 95, 946-957 (1984).

(15) NASA Technical Paper 1464, **Application of Space Technology to Crustal Dynamics and Earthquake Research** (1979); R. J. Coates, H. Frey, G. D. Mead, J. Bosworth, **The NASA Crustal Dynamics Project**, preprint (1984).

(16) G. A. Thompson and D. B. Burke, Geol. Soc. Amer. Bull. **84**, 627-632 (1973).

(17) R. W. Greensfelder, F. C. Kintzner, M. R. Somerville, Geol. Soc. Amer. Bull. **91**, 518-523 (1980).

(18) J. K. Crouch, S. B. Bachman, J. T. Shay, in **Tectonics and Sedimentation along the California Margin**, J. K. Crouch and S. B. Bachman, Eds. (Pacific Sect. Soc. Econ. Paleontol. Mineral. **38**, 1984), pp. 17-34.

(19) R. O. Burford, in **Proc. 2nd Internat. Symposium on Recent Crustal Movements** (Aulanko, Finland, 1965), pp. 100-110; R. O. Burford, **Strain Analysis Across the San Andreas Fault and Coast Ranges of California**, Ph.D. Thesis, Stanford University, Stanford, California (1967).

(20) W. J. Gawthrop, in **San Gregorio-Hosgri Fault Zone, California**, E. A. Silver and W. R. Normark Eds. (Calif. Div. of Mines and Geol. Spec. Rep. **137**, 1978), pp. 45-56.

(21) J. H. Stewart, in **Cenozoic Tectonics and Regional Geophysics of the Western Cordillera**, R. B. Smith and G. P. Eaton Eds., (Geol. Soc. Amer. Mem. 152, 1978), pp. 1-13; also G. A. Davis, in **Continental Tectonics**, (Nat. Acad. Sci., Washington, D. C., 1980), pp. 84-95.

(22) R. E. Wallace, U. S. Geol. Surv. Open-File Rep., 78-94 (1978); also J. Geophys. Res. **89**, in press (1984).

(23) C. A. Hall, Jr., Science **190**, 1291-1294 (1975); S. A. Graham and W. R. Dickinson, Science **199**, 179-181 (1978).

(24) C. A. Hall, Jr., J. Geophys. Res. **86**, 1015-1031 (1981).

(25) G. E. Weber and K. R. Lajoie, Geol. Soc. Amer. Abstr. with Prog. 9, 524 (1977).

(26) This research was supported by the National Aeronautics and Space Administration, under NASA's Crustal Dynamics Project.

APPENDIX 3:

Reduction of Space-Geodetic Vector Position Data: Rate Scaling of Global Plate Tectonic Models

by

Mark H. Murray

under the superivison of
Thomas H. Jordan

December 1985

Abstract

Satellite laser ranging observations to Lageos during 1978-1983 are used to analyze the vector rate-of-change of annual station positions for comparison with global plate tectonic models. We develop an algorithm suitable for the reduction of large, inhomogeneous space-geodetic data sets, which accounts for the full position covariances, and coordinate transformations between epochs. Tectonic motions are isolated by reducing systematic errors in radial position determination and contaminations due to errors in earth-orientation parameters. This is accomplished by forming a linear system of equations which describe differenced station position vectors as a combination of tectonic motion model parameters, and nuisance parameters which comprise non-tectonic motions such as rigid-body rotations. The system is normalized with the square-root of the covariance matrix, and then rendered insensitive to the nuisance parameters by the application of projection operators. Model parameters are estimated from the resulting reduced system by generalized-inverse techniques. This methodology is applied to the problem of rate scaling of global plate tectonic models. The model is parameterized by $\gamma \mathbf{m}_o$, where $\mathbf{m}_o$ is an *a priori* model of tangential relative velocity vectors, such as RM2; thus, $\gamma = 1$ implies that the mean rate of motion of the observing stations is identically equal to the RM2-predicted rates. We find $\gamma = 0.95 \pm 0.16$, indicating that the mean rate of SLR-derived motions for a five-year interval are consistent with RM2, which is averaged over a 2-m.y. interval. We find that the data do not place significant constraints on possible errors in marine magnetic anomaly timescales, but are not consistent with an interval of quiescent or accelerated plate motions.

Introduction

Satellite laser ranging (SLR) and very-long baseline interferometry (VLBI) are space-geodetic techniques currently capable of determining relative locations of widely separated positions on the earth's surface to within sub-decimeter accuracy (Shapiro, 1983). Results from interferometry with the Global Positioning System (GPS) are achieving similar accuracies (Bock *et al.*, 1985). This capability raises the possibility of detecting and monitoring relative plate motions and deformations. Analysis of the rate of change of baseline length between many station positions are in good agreement with predictions based on global plate tectonic models (e.g. Smith *et al.*, 1979; Christodoulidis *et al.*, 1985; Tapley *et al.*, 1985; Clark *et al.*, 1985), although some significant discrepancies do exist (e.g. Minster and Jordan, 1984). These treatments of space-geodetic data concentrate on the scalar baseline lengths, which are relatively insensitive to systematic errors due to coordinate transformations between epochs. However, the data are intrinsically three-dimensional. Thus, if the errors can be removed or reduced in a systematic manner, an analysis of the rate of change of the geocentric position *vector* could provide additional insight, especially with regard to directions of motion. As these data sets grow, the need for efficient algorithms capable of handling large, inhomogeneous, multiple-epoch data sets becomes increasingly critical. In this paper, we present the nucleus of such an algorithm, and then, using data derived from laser ranging to the Lageos satellite, we apply this algorithm to the problem of rate scaling of global plate tectonic models.

We first examine the nature of the satellite laser ranging data and some of its inherent difficulties. In May 1976, Lageos (Laser Geodynamics Satellite) was launched into a nearly circular orbit at an elevation of 5900 km and an inclination of 109.8° to the equatorial plane. The satellite is a sphere 60 cm in diameter, weighing

411 kg, and is covered with 426 retroreflectors. The satellite's design and orbit minimize the forces due to solar radiation pressure, earth albedo, and atmospheric drag, and thus, Lageos very nearly defines an artifical reference frame in earth orbit. Ground-based laser systems measure the round-trip pulse propagation time and, using an adopted value for the speed of light, calculate the range. In theory, if the satellite's position is known perfectly, the location of the laser site may be determined after a number of ranges have been obtained. In practice, of course, the problem is considerably more difficult. Since ranges to Lageos, in general, are not made simultaneously, the orientation of the earth with respect to the satellite reference frame must be determined for the time of the observation. This requires knowledge of a complex set of motions which include earth precession, nutation, polar motion, and rotation, as measured by UT1. The satellite's position is controlled by the external forces which act upon it; these include the earth's gravity field, luni-solar and planetary gravity fields, solid-earth and oceanic tides, solar radiation, and earth albedo. Range measurements are affected by refraction of the laser pulse in the atmosphere, tidal displacements, pulse detection accuracy, and are scaled by the adopted value for the speed of light. Thus, the accuracy of the station positions depends critically upon the accuracy of the earth-orientation, force, and measurement models. One such set of models and the procedure for reducing raw range values to station position coordinates used by Goddard Space Flight Center is called SL5.1AP, and is described in Christodoulidis *et al.* (1985), and Smith *et al.* (1985). The data that we utilize is derived from an improved set of models, denoted by SL6, and are solutions for annual geocentric vector positions and covariances derived from observations of Lageos between 1978 and 1983.

Methodology

We now consider the problem of constraining plate tectonic motions and deformations from space-geodetic networks. Ideally, the analysis procedures should be capable of handling data derived from disparate techniques such as SLR, VLBI, and GPS simultaneously, taking into account the coordinate transformations and scaling parameters particular to each. For example, the natural coordinate system for SLR has an origin at the earth center of mass, whereas VLBI uses an origin at the solar system barycenter; also, SLR, unlike VLBI, is sensitive to the adopted value of the earth gravitational mass. Any estimation of parameters by inversion techniques should account for possible errors in the data, therefore the analysis must incorporate the full covariance matrix corresponding to the data. Another potential problem arises from non-uniform sampling of network stations from epoch to epoch. Usage of homogeneous data sets, i.e. including only stations that are sampled during every epoch, is often too restrictive and ignores important sources of information. However, inhomogeneous sampling may introduce biases in the estimation of station parameters due to changing network geometry, which result in unequal weighting between successive epochs. For example, one epoch may preferentially sample "fast" plates. The approach we have taken is similar to that used by Jordan and Sverdrup (1981) for the estimation of earthquake location, whereby we form a linear system of equations which describe differenced station position vectors as a combination of tectonic motion model parameters and nuisance parameters, which comprise non-tectonic motions such as rigid-body rotations. The system is normalized with the square-root of the covariance matrix, and then rendered insensitive to the nuisance parameters via application of projection operators, a process which we term "denuisancing".

Let us consider a simplified algorithm tailored to the specific problems presented by SLR observations. First, if all the data is processed in a consistent manner, such as with the SL6 model, scaling of the network due to the adopted value for the speed of light will be uniform and hence negligible. Similarily, the earth center of mass, which is an implicit function of the assumed gravity model, is constant for all epochs. Thus, representation of scaling or transformation of coordinate systems may be safely ignored. Errors in earth-orientation parameters, such as polar motion and UT1, will result in rigid-body rotation of the entire network about the earth center of mass. However, absolute plate motions, which are relative plate motions defined in a particular angular velocity reference frame, will tradeoff exactly with rigid-body rotations. Therefore, we may only resolve relative plate motions from the data and will treat rigid-body rotations as nuisance parameters. Some provision should be made for differences between errors in site motion tangential and radial to the surface of the earth, which arise from inhomogeneous sampling of ranges. For example, lasers may range at all horizontal azimuths, but may not range at vertical angles below the horizon; thus, systematic errors in satellite location and in the atmospheric refraction model are expected to map primarily into the radial components of position. Therefore, radial components may also need to be treated as nuisance parameters. Finally, tectonic motions may bias the denuisancing of rotations, since incomplete sampling of the plate system might introduce rotations of tectonic origin. This subtle problem may be minimized if prior information about the motions is known; the *a priori* tectonic model is subtracted from the data before denuisancing, and then is added to the resulting model after the inversion has been completed. This process, which we term "bias stripping", causes the component of the solution which is not constrained by the data to coincide with the *a priori* model, thus care must be exercised in the choice of the *a priori* model.

With these considerations in mind, we may formulate a specific approach. We

define x to be a vector composed of the three-component geocentric vector station positions for all stations sampled during all epochs under study. These positions will have associated covariances defined by $\hat{V}_x = \langle (x-\langle x \rangle) \cdot (x-\langle x \rangle)^T \rangle$, where the brackets denote expected value, and the T transpose. x and $\hat{V}_x$ are the quantities supplied by the SL6 solution. This covariance matrix is not an accurate reflection of the true errors associated with the station coordinates due to systematic errors in the normal point ranges used to derive the SL6 solution. Normal points are formed by grouping raw ranges to Lageos from a laser site into 2 minute bins, and then finding average ranges from those samples; this data compression, which can typically be two orders of magnitude, is useful computationally and reduces biases due to uneven sampling of the orbit of Lageos. The precision of ranges is on the order of 2-9 cm, and thus the formal precision of the normal points is generally on the order of 1 cm or less. However, due to systematic orbit model errors, which propagate as the square of time, the actual accuracy of the normal points is more on the order of 10-15 cm over a 30 day orbital arc. To reconcile this problem, SL6 uniformly assigns each normal point a formal uncertainty of 100 cm, which means that the stated covariances are probably an overestimation of the errors. A more realistic estimate of covariance might be $V_x = \nu^2 \hat{V}_x$, where ν^2 is a scalar to be determined *a posteriori* by the sampling variance, which is a function of the weighted error vector and the number of degress of freedom.

We define

$$\mathbf{d} = \mathbf{E} \cdot \mathbf{x} \tag{1a}$$

$$\hat{V}_d = E \cdot \hat{V}_x \cdot E^T \tag{1b}$$

where **E** is the operator composed of 1's, 0's, and -1's which difference vector positions between successive epochs for all sampled stations. **d** therefore represents

the apparent vector motions of the stations from epoch to epoch. Based on the previous discussion, we consider a decomposition of these motions into rigid-body rotations, tectonic motions, such as rigid plate motions and internal plate deformations, radial motions and errors. We construct a linearized set of equations of the form:

$$\mathbf{A} \cdot \mathbf{m} + \mathbf{B} \cdot \mathbf{n} = \mathbf{d} \qquad (2)$$

where $\mathbf{m}$ is a vector composed of model parameters corresponding to tectonic motions, and $\mathbf{n}$ is a vector composed of nuisance parameters. The particular representation of these vectors will depend on the desired parameterization. For example, if rigid-body rotations are to be denuisancēd from the system, $\mathbf{n}$ will be composed of the three-component angular velocity vectors corresponding to the rotations between successive epochs, and $\mathbf{B}$ will be composed of the 3x3 anti-symmetric infinitesimal rotation matrices times the epoch-time differences for each station sampled. $\mathbf{m}$ may be the denuisanced vectors of motion, in which case $\mathbf{A}$ will be the identity matrix; or, as discussed in the following section, $\mathbf{m}$ may be a rate-scaling parameter and $\mathbf{A}$ the vectors corresponding to an *a priori* global plate tectonic model. Explicit representations of these matrices will be given for the specific application of rate scaling of global tectonic models; however, we wish to emphasize that this is a completely general formulism capable of handling many possible parameterizations, provided the system is linear or can be linearized.

We normalize the system by weighting with the square-root of the covariance matrix

$$\hat{\mathbf{A}} \cdot \mathbf{m} + \hat{\mathbf{B}} \cdot \mathbf{n} = \hat{\mathbf{d}} \qquad (3)$$

where $\hat{\mathbf{A}} = \hat{\mathbf{V}}_d^{-1/2} \cdot \mathbf{A}$, etc.; note that the carat now indicates normalization by

$\hat{V}_d^{1/2}$. The system is denuisanced by applying

$$Q_B = I - \hat{B} \cdot \hat{B}^{\dagger}, \tag{4}$$

where the dagger denotes the Moore-Penrose generalized inverse (Penrose, 1955). Q_B is the projection operator which projects (3) into the null space of $\hat{B}^T$, thus rendering the system insensitive to the nuisance parameters; it is both symmetric and idempotent ($Q_B = Q_B^T = Q_B \cdot Q_B$). Multiplying both sides of (3) by (4), and making use of the fact that $Q_B \cdot \hat{B} = 0$, we find

$$Q_B \cdot \hat{A} \cdot m = Q_B \cdot \hat{d}. \tag{5}$$

The model parameters are estimated by taking the generalized inverse of the left hand side of the reduced system (5)

$$\tilde{m} = (Q_B \cdot \hat{A})^{\dagger} \cdot Q_B \cdot \hat{d}, \tag{6}$$

with the associated unscaled covariance matrix

$$\hat{V}_m = (Q_B \cdot \hat{A})^{\dagger} \cdot Q_B \cdot (Q_B \cdot \hat{A})^{\dagger T} \tag{7a}$$

$$= (\hat{A}^T \cdot Q_B \cdot \hat{A})^{\dagger}. \tag{7b}$$

We now estimate the covariance scaling parameter v^2 by comparing the misfit between the model and the data; this is defined by the normalized error vector, which is a random variable found by substituting (6) into (5):

$$\hat{e} = Q_B \cdot \hat{d} - Q_B \cdot \hat{A} \cdot \tilde{m} \tag{8a}$$

$$= (I - (Q_B \cdot \hat{A}) \cdot (Q_B \cdot \hat{A})^{\dagger}) \cdot Q_B \cdot \hat{d}. \tag{8b}$$

The squared length of the normalized error vector divided by the covariance scaling parameter is itself a random variable and is chi-squared distributed with N-M degrees of freedom, where N is the rank of the reduced data space $Q_B \cdot \hat{\mathbf{d}}$, and M is the rank of the projection operator $(Q_B \cdot \hat{\mathbf{A}}) \cdot (Q_B \cdot \hat{\mathbf{A}})^{\dagger}$ (e.g., Jordan and Sverdrup, 1981). Thus, it has the expected value

$$< \hat{\mathbf{e}}^T \cdot \hat{\mathbf{e}} > / \nu^2 = N - M. \tag{9}$$

The observed misfit is one realization of this error process, and can thus be used to estimate ν^2. This estimate is called the normalized sampling variance:

$$\hat{s}^2 = \hat{\mathbf{e}}^T \cdot \hat{\mathbf{e}} / (N-M). \tag{10}$$

Application of bias stripping is a simple extension of the method outlined above. Let $\mathbf{m}_o$ be the *a priori* model which is assumed to be known perfectly; that is, let $\mathbf{m}_o$ have zero variance ($\mathbf{m}_o = < \mathbf{m}_o >$). The *a priori* model is removed from the linear system (2):

$$\mathbf{A} \cdot (\mathbf{m} - \mathbf{m}_o) + \mathbf{B} \cdot \mathbf{n} = \mathbf{d} - \mathbf{A} \cdot \mathbf{m}_o. \tag{11}$$

The equations are normalized with the square-root of the covariance matrix in (1), since $\mathbf{m}_o$ has zero variance, and applying the appropriate denuisancing and generalized-inverse techniques, we find the estimate of the model parameters

$$\tilde{\mathbf{m}} = \mathbf{m}_o + (Q_B \cdot \hat{\mathbf{A}})^{\dagger} \cdot Q_B \cdot (\hat{\mathbf{d}} - \hat{\mathbf{A}} \cdot \mathbf{m}_o) \tag{12a}$$

$$= (Q_B \cdot \hat{\mathbf{A}})^{\dagger} \cdot Q_B \cdot \hat{\mathbf{d}} + (\mathbf{I} - (Q_B \cdot \hat{\mathbf{A}})^{\dagger} \cdot (Q_B \cdot \hat{\mathbf{A}})) \cdot \mathbf{m}_o. \tag{12b}$$

It is straightforward to show that the unscaled covariance matrix, the normalized error vector, and the sampling variance are given by (7), (8), and (10) respectively; this follows from the fact that $\mathbf{m}_o$ has zero variance. The first term in (12b) is equivalent to (6), the result obtained with bias stripping. The second term projects $\mathbf{m}_o$ into the model space which is unconstrained by the data. Thus, the component of the model which is not constrained by the data is made to coincide with the *a priori* model.

We have described a very general approach for the estimation of model parameters and variance scaling in the presence of nuisance parameters. We now apply the methodogy outlined above to the specific problem of the rate scaling of global plate tectonic models.

Rate Scaling of Global Plate Tectonic Models

As an introduction to this problem, we briefly describe one successful model of plate tectonic motions obtained by Minster and Jordan (1978), hereafter denoted by RM2. RM2 is a relative motion model based on the assumption that the earth's surface is composed of eleven plates which are rigid spherical caps moving tangentially to the surface. Directions of motion are estimated from azimuths of transform faults and earthquake slip vectors, and rates of motion are estimated from marine magnetic anomalies. No data are used from locations where the assumptions do not appear to be valid, such as regions of deformation at continent-continent boundaries. Magnetic anomalies 2, 2', and, occasionally, 3 are employed, thus the obtained rates are averaged over a 2-m.y. interval. One-sigma errors for the rates are on the order of 5 to 10%.

As an application of the algorithm decribed in the previous section, we estimate

from the SL6 solution the RM2 rate-scaling parameter γ. That is, we assume that the orientation of the relative angular velocity vector for each pair of plates is known perfectly and that the rate of rotation is of the form $\gamma\omega$, where ω is the RM2 angular rate of rotation. Thus, the *relative* magnitude of the RM2 rates are assumed to be known perfectly, but they may be scaled according to γ. For example, $\gamma = 1$ implies that the relative velocities of the observing stations are identically equal to the RM2-predicted values, whereas $\gamma < 1$ implies that the observed mean rates are slower than RM2. Thus, we seek to characterize the data by a single model parameter. Such a characterization maximizes the resolution of the model parameter at the expense of greater variance. As such, it represents a logical first assessment of the data, and will help to ascertain the appropriateness of RM2 as an *a priori* bias-stripping model. The rate-scaling parameter γ is a useful description of mean global plate motion, and facilitates comparison of mean rate estimates derived from geophysical and geodetic techniques representing timescales over many orders of magnitude. The utility of such comparisons will depend on the assumption that the relative directions of plate motion do not change substantially over the averaging interval. For example, estimations based on plate reconstructions over the last 80 m.y. (e.g., Davis and Solomon, 1981) which include major reörganization of plate geometry, are possible, but will be degraded due to poorly-matched motions. RM2 provides a reference estimate of γ based on marine magnetic anomalies averaged over a 2-m.y. interval, whereas space-geodetic data offer independent estimates which sample the last 10 years.

We now adapt the methodology of the previous section to the problem of estimating γ from SLR data. Let $\mathbf{d}$ be the vector composed of the SL6-derived geocentric vector station motions, with associated covariance $\hat{\mathbf{V}}_d$, as given by (1). To compare $\mathbf{d}$ to RM2-predicted tangential motions, we must reduce biases due to rigid-body rotations and radial motions from the data. An infinitesimal geocentric

rigid-body rotation may be represented by $\rho \cdot \Omega$, where Ω is a three-component rotation vector, and ρ is the 3x3 anti-symmetric matrix

$$\rho = \begin{bmatrix} 0 & z & -y \\ -z & 0 & x \\ y & -x & 0 \end{bmatrix} \tag{13}$$

where x,y,z are the nominal cartesian station coordinates (e.g., Goldstein, 1980). We define **B** to be composed of the ρ_i's corresponding to motion of the ith station, and **n** be composed of the Ω_{jk}'s corresponding to motion between the jth and kth epochs; in this way, the rigid-body rotations described by **n** may be treated as nuisance parameters. The assumption of infinitesimal rotation is valid for the observed centimeter motions; such rotations are additive, allowing data from inhomogeneously sampled networks to be fully utilized in a simultaneous inversion over all sampled epochs. For example, for a two station network where station 1 is observed during three epochs, and station 2 is observed in the first and last epochs, we would define

$$\mathbf{B} \cdot \mathbf{n} = \begin{bmatrix} \rho_1 & 0 \\ 0 & \rho_1 \\ \rho_2 & \rho_2 \end{bmatrix} \cdot \begin{bmatrix} \Omega_{12} \\ \Omega_{23} \end{bmatrix} \tag{14}$$

To remove radial components of motion and all covariances between tangential and radial motions, we convert from geocentric to local geodetic coordinates via the transformation matrix **J**, which has jacobian block diagonal elements corresponding to the nominal station positions, and isolate the local north and east components of motion by removing the rows and columns corresponding to vertical components via the tangential selection matrix **T**, which is simply composed of 1's and 0's.

Thus, we define

$$\mathbf{d}' = \mathbf{F} \cdot \mathbf{d} \tag{15a}$$

$$\hat{\mathbf{V}}_{d'} = \mathbf{F} \cdot \hat{\mathbf{V}}_{d} \cdot \mathbf{F}^{T} \tag{15b}$$

$$\mathbf{B}' = \mathbf{F} \cdot \mathbf{B} \tag{15c}$$

where $\mathbf{F} = \mathbf{T} \cdot \mathbf{J}$. Because of the linear relationship between local geodetic velocities and angular rate of rotation (Minster *et al.*, 1974), we may parameterize the model by $\gamma \mathbf{m}_o$, where $\mathbf{m}_o$ is the vector composed of predicted RM2-derived velocities in local geodetic coordinates multiplied by the time difference between the epochs. The RM2 velocities are calculated with respect to a fixed plate; the choice of the fixed plate is arbitrary since it results in a rigid-body rotation the network which is removed by application of $\mathbf{Q}_B$, as given in (5). Thus, we may define the system:

$$\gamma \mathbf{m}_o + \mathbf{B}' \cdot \mathbf{n} = \mathbf{d}'. \tag{16}$$

Noting the equivalence of (16) to (2), where $\gamma = \mathbf{m}$, and $\mathbf{m}_o = \mathbf{A}$, we find from (6):

$$\tilde{\gamma} = (\mathbf{Q}_{B'} \cdot \hat{\mathbf{m}}_o)^{\dagger} \cdot \mathbf{Q}_{B'} \cdot \hat{\mathbf{d}}' \tag{17}$$

which, being scalar, has unscaled variance, given by (7)

$$\hat{\sigma}_{\gamma}^{2} = (\hat{\mathbf{m}}_o^{T} \cdot \mathbf{Q}_{B'} \cdot \hat{\mathbf{m}}_o)^{\dagger} \tag{18}$$

and ν^2 is estimated from (8) and (10).

This method does not account for possible biases in model estimation due to tectonic motion; we previously suggested that such contaminations might be reduced by bias stripping with an *a priori* model of tectonic motion. It is straightforward to show, however, that this procedure is applied implicitly when estimating the

rate-scaling parameter. Define $\gamma(\alpha) = \delta\gamma + \alpha$, where α is a constant. We bias strip using $\alpha\,\mathbf{m}_o$ as the *a priori* model; thus, $\alpha = 0$ corresponds to no bias stripping, and $\alpha = 1$ is equivalent to bias stripping with $\mathbf{m}_o$. Then (16) becomes

$$\delta\gamma\,\mathbf{m}_o + \mathbf{B}'\cdot\mathbf{n} = \mathbf{d}' - \alpha\,\mathbf{m}_o \tag{19}$$

It follows that

$$\tilde{\delta\gamma} = (\mathbf{Q}_{B'}\cdot\hat{\mathbf{m}}_o)^{\dagger}\cdot\mathbf{Q}_{B'}\cdot\hat{\mathbf{d}}' - \alpha\,(\mathbf{Q}_{B'}\cdot\hat{\mathbf{m}}_o)^{\dagger}\cdot\mathbf{Q}_{B'}\cdot\hat{\mathbf{m}}_o \tag{20}$$

and

$$\tilde{\gamma}(\alpha) = (\mathbf{Q}_{B'}\cdot\hat{\mathbf{m}}_o)^{\dagger}\cdot\mathbf{Q}_{B'}\cdot\hat{\mathbf{d}}' + \alpha\,[1 - (\mathbf{Q}_{B'}\cdot\hat{\mathbf{m}}_o)^{\dagger}\cdot\mathbf{Q}_{B'}\cdot\hat{\mathbf{m}}_o] \tag{21}$$

Note that $(\mathbf{Q}_{B'}\cdot\hat{\mathbf{m}}_o)^{\dagger}\cdot\mathbf{Q}_{B'}\cdot\hat{\mathbf{m}}_o$ is an idempotent scalar projection operator, and must equal either 0 or 1. $\mathbf{Q}_{B'}\cdot\hat{\mathbf{m}}_o$ is the relative motion model in a no net-rotation frame; for non-trivial cases this will be non-zero and therefore the projection operator equals 1. The quantity in the square brackets of (21) vanishes and we find the estimate of the rate-scaling parameter is not a function of α; hence, bias stripping is implicitly contained in this particular formulation.

The nominal station positions (shown in Figure 1) and distribution of normal points for the stations used in the estimation of the rate-scaling parameter are listed in Table 1; the inhomogeneous sampling of network geometry which is evident from this distribution provides some justification for the multiple-epoch denuisancing procedures described above. The data, which consist of 52 local geodetic motion vectors corresponding to 23 stations sampled over 6 epochs (1978-1983), are listed in Table 2; coverage includes 5 of the 11 RM2-defined plates. These vectors with their associated tangential error ellipses (1 sigma, unscaled) are shown in Figure 2; this figure provides some sense of the distribution and quality of the formal errors of the data--it does not portray the often significant covariance between station motions.

Applying the above methodology to the complete five-year interval data set, we

obtain:

$$\tilde{\gamma} = 0.95 \pm 0.16 \quad \text{(one sigma)}.$$

The one-sigma level of confidence is obtained from $\hat{s}^2 = 0.355$, and $\hat{\sigma}_\gamma^2 = 0.072$. Additional estimations based on epoch-subsets are listed in Table 3; for example, using all the stations with data in both 1982 and 1983, which we denote {5,6}, the one-year interval estimate of γ is 0.51 ± 0.50. These results are plotted as a function of the number of data vectors utilized in each solution in Figure 3. In all but four cases, the SLR-derived rate-scaling parameter is consistent with the RM2-reference value (γ = 1) at the one-sigma level of confidence. One exception, {3,4,5}, is very nearly consistent (1.275 ± 0.270), and the remaining exceptions ({1,2}, {1,2,3}, {1,2,3,4}) all include data from the first epoch, 1978. This epoch was sparsely sampled, using measurement techniques which have been subsequently refined; it is therefore possible that these data may be subject to systematic errors not accounted for by SL6. If the 1978 data is ignored, estimates of the rate-scaling parameter averaged over a one-year interval vary between 0.44 and 1.31, and show less variability for longer intervals. In summary, we find that the SLR-derived mean rate of motion among the observing stations for a five-year averaging interval, and even for intervals as short as one year, are consistent with RM2.

Discussion

This result supports previous scalar baseline rate-of-change analyses indicating that the direct measurement of plate tectonic motions is feasible using space-geodetic techniques (e.g., Christodoulidis *et al.*, 1985); however, we find that an analysis of the

vector motions associated with network station position provides additional information and constraints on "instantaneous" plate motions. For example, the use of RM2 as an *a priori* model of tectonic motion appears to be reasonably justifiable, as the improvement in results for longer averaging interval indicates. It should be noted that estimation of the rate-scaling parameter assumed that RM2 is known perfectly with the exception of the absolute magnitude of the rates. In reality, RM2 is a model with associated covariance due to errors in azimuths and magnetic anomalies; however, the errors associated with RM2 are small compared to those of SLR data, and therefore are not likely to make any substantial contribution to the estimation of the rate-scaling parameter. Further experimentation with alternative *a priori* models which may provide additional improvements, such as NUVEL-1 (Demets *et al.*, 1985), should, of course, be pursued. As data coverage becomes more extensive, global plate tectonic models based solely on space-geodetic data may ultimately supplant those based on less instantaneous data; these improved models will help to reduce biases in the estimation of model parameters.

Another notable feature of this vector analysis is the estimation of the sampling variance $\hat{s}^2 = 0.355$. Previous estimates of the sampling variance, which have been on the order of 0.10 to 0.15 (D. Smith, private communication), have relied on the analysis of single scalar baseline lengths, under the assumption that additional variances corresponding to other baselines, even if they are larger, will not increase the overall variance of the system. This assumption is valid provided the variances are uncorrelated. This is not the case for the SLR data; use of the full covariance matrix as well as a unified algorithm which considers all the data simultaneously indicate that the previous estimates of sampling variance are too small by a factor of 2 or 3.

We now consider some of the broader geophysical implications of these results. We have found that the SLR-derived mean global plate rates for a 5-year interval

agree with the 2-m.y. average RM2 rates; this suggests possible limitations for the temporal variability of mean global motion. Anderson (1975) proposed that observed tectonic motions in the vicinity of plate boundaries, such as subduction zone trenches, may be relatively stationary for long periods (30-100 yr), except for brief (5-10 yr) "breaking cycles" in which the accumulated stress along the boundary is released. During such a cycle, the plate motions near the boundary are accelerated. Episodic motion at plate boundaries is, of course, well documented; Anderson, from observations of seismic migration patterns such as the Aleutian sequence between 1899 and 1905, suggested these episodic motions are correlated and that the compression of the oceanic lithospheric plate between breaking cycles may extend well into the interior of the plate. One possible implication of this model is that global plate motions may be "jerky"; that is, quiescent except for relatively short periods of accelerated motions. The five-year SLR-derived mean rate of motion is not consistent with either a quiescent, or accelerated interval of plate motions. One-year estimates display graeater variablilty but are, with the exception of the 1978 data, also consistent with RM2. Possible interpretations of systematic temporal variations must be regarded with some skeptism due to the sparcity of data, and to the previously-mentioned systematic improvements in data collection techniques which may not be accurately modeled by SL6. Clearly, many additional years of space-geodetic data collection are required before strong constraints may be placed on temporal variation in mean plate motion.

The sampling frequency of the SLR data severely restricts efforts to make interpretations regarding longer averaging intervals; this point is illustrated in Figure 4 which shows estimates of global rate-scaling parameter as a function of the sampling interval. Space-geodetic data provide the most recent estimates averaged over the shortest intervals; it is easily possible to imagine temporal variations of motion over the entire spectrum of timescales out to 2 m.y. or more. For example,

Vogt (1985) suggests, from a detailed examination of the magnetic lineations at six accreting plate boundaries, that opening rates have been up to 7-35% faster over the last 1 m.y. than over the period 1-2 m.y. Other geological techniques may provide crude estimates for timescales intermediate between space-geodetic and marine magnetic anomaly intervals. Estimates of slip rate at plate boundaries based on paleoseismicity, such as those obtained by trenching on the San Andreas Fault by Sieh and Jahns (1984), sample averaging intervals of 1000-10000 years. A robust estimate of γ would require many such estimates of slip rate over the same time period; the natural paucity of suitable sites will hinder such an effort. Furthermore, the rates obtained by Sieh and Jahns (1984) are consistent with more recent geodetic estimates but show a large discrepancy with RM2 rates; Minster and Jordan (1984) suggest that distributed deformation both east and west of the San Andreas may account for this discrepancy. Thus, care must be exercised when measurements obtained at plate boundaries are used to estimate global plate motion. Despite such obstacles, the variability of the rate-scaling parameter over different timescales warrants further investigation, because such variations might be a reflection of the dynamical processes which drive the observed plate motions.

As has been noted, RM2 rates are derived from observations of marine magnetic anomalies; errors in the magnetic anomaly timescale will therefore result in scaling errors of the RM2 rates. Under the assumption that global plate motion has been nearly uniform over the last 3 m.y., space-geodetic data offer an independent constraint on possible errors in the magnetic anomaly timescale. RM2 uses the magnetic anomaly timescale of Talwani *et al.* (1971) for the estimation of the age of anomalies 2, 2' and 3. In a more recent compilation of anomaly timescales, Ness *et al.* (1980) point out several disadvantages of the Talwani scale. First, it was obtained from profiles over the Reykjanes Ridge, which is a slow spreading ridge; such profiles tend to have poorer resolution due to contamination of normal and reversed blocks from

subsequent flows. Second, it is a hybrid scale, constructed by assuming the age of the end of anomaly 5 (9.94 m.y.) of Heirtzler *et al.* (1968) to be correct, assigning residuals from the Heirtzler scale to be due to errors in that scale, and then compromising on the age of the 3.1' anomaly from considerations of magnetostratigraphy. Finally, it does not incorporate the change in K-Ar decay and abundance constants suggested by the International Union of Geological Sciences in 1977; this change alone would result in a 2.68% decrease in RM2 rates (Mankinen and Dalrymple, 1979). Ness *et al.* (1980) propose a new anomaly timescale which displays systematic differences with the Talwani scale. Table 4 compares the chronologies, and the corresponding rate-scaling parameter obtained by dividing the age from the Talwani scale by teh age from the Ness scale. These estimates of γ are shown in Figure 4. The variability of these estimates provides some measure of the possible errors in the RM2 marine magnetic anomaly timescale; we find that the variations lie well within the formal error bars of the SLR-derived estimate. Although there are indications that the anomaly timescale used to determine the RM2 rates may be in error, the quality of the SL6 data set is not at present sufficient to place useful constraints on that error.

Conclusions

We have developed a general methodology for the analysis of space-geodetic data with the goal of constraining plate tectonic motions. The generalized-inverse analysis of the vector rate-of-change of the geodetic network accounts for the full covariance of the station motions and reduces contaminations due to rigid-body rotations and poorly-constrained vertical motions. We have demonstrated the applicability of these algorithms to obtain the RM2 rate-scaling parameter, which we believe to be a useful description of mean global plate motion worthy of further investigation via other geophysical and geological techniques. An estimate of the

rate-scaling parameter from a five-year interval of laser ranging to the Lageos satellite is found to be near unity and consistent with RM2 rates. There is a suggestion that the magnetic anomaly timescale on which RM2 is based predicts faster rates than more recent timescales, but SLR data do not as yet place any constraints on this error. In addition, the mean rate of motion of the plates argues against the suggestion that the plates are in a period of quiescent, or accelerated motion.

An obvious extension of this analysis would be the inclusion of VLBI data which presently offer useful network stations in Europe. More complicated parameterizations of the model are under consideration. Examination of vertical motions would provide a further test of consistency, and might indicate areas of active deformation. Grouping the stations by assumed plate might yield constraints on the directions of tectonic motions, as well as the stability of the plates themselves. Allowing individual stations to move with constant velocity might reveal anomalous behavior at plate boundaries. Space-geodetic datasets have begun to place useful constraints on global plate motions. It is clear, however, that efficient algorithms to handle the rapidly accumulating space-geodetic data, which are capable of treating the problems associated with each technique in a self-consistent manner, will be crucial for the detection and monitoring of temporal variations in plate motions.

References

Anderson, D. L., Accelerated plate tectonics, *Science*, 1[illegible], 1077-1079, 1975.

Bock, Y., R. I. Abbot, C. C. Counselman III, S. A. Gourevitch, and R. W. King, Establishment of three-dimensional geodetic control by interferometry with the Global Positioning System, *J. Geophys. Res.*, **90**, 7689-7703, 1985.

Christodoulidis, D. C., D. E. Smith, R. Kolenkiewicz, S. M. Klosko, M. H. Torrence, and P. J. Dunn,Observing tectonic plate motions and deformation from satellite laser ranging, *J. Geophys. Res.*, **90**, 9249-9264, 1985.

Clark, T. A., B. E. Corey, J. L. Davis, G. Elgered, T. A. Herring, H. F. Hinteregger, C. A. Knight, J. I. Levine, G. Lundqvist, C. Ma, E. F. Nesman, R. B. Phillips, A. E. E. Rogers,B. O. Ronnang, J. W. Ryan, B. R. Schulpler, D. B. Shaffer, I. I. Shapiro, N. R. Vandenberg, J. C. Webber, and A. R. Whitney, Precision geodesy using the Mark-III very-long baseline interferometry system, *IEEE Trans. on Geoscience and Remote Sensing*, **GE-23**, 438-449, 1985.

Davis, D. M., and S. C. Solomon, Variations in the velocities of the major plates since the late Creataceous, *Tectonophysics*, **74**, 189-208, 1981.

Demets, C., R. G. Gordon, S. Stein, D. F. Argus, F. Engeln, P. Lundgren, D.G. Quible, C. Stein, S. A.Weinstein, D. A. Weins, D. F. Woods, NUVEL-1: A new global plate motion dataset and model (abstract), *EOS Trans. AGU*, **66**, 368-369, 1985.

Goldstein, H., *Classical Mechanics*, 2nd. ed., Addison-Wesley, Reading, Massachusetts, 672 pp., 1980.

Heirtzler, J. R., G. O. Dickson, E. M. Herron, W. C. Pitman III, and X. LePichon, Marine magnetic anomalies, geomagnetic field reversals, and motions of the ocean floor and continents, *J. Geophys. Res.*, **73**, 2119-2136, 1968.

Jordan, T. H., and K. A. Sverdrup, Teleseismic location techniques and their application to earthquake clusters inthe south-central Pacific, *Bull. Seism. Soc. Am.*, **71**, 1105-1130, 1981.

Mankinen, E. A., and G. B. Dalrymple, Revised geomagnetic polarity time scale for the interval 0-5 m.y. B.P., *J. Geophys. Res.*, **84**, 615-626, 1979.

Minster, J. B., and T. H. Jordan, Present-day plate motions, *J. Geophys. Res.*, **83**, 5331-5354, 1978.

Minster, J. B., and T. H. Jordan, Vector constraints on Quaternary deformation of the Western United States east and west of the San Andreas Fault, in *Tectonics and Sedimentation along the California Margin*: Pacific Section, S. E. P. M., Crouch, J. K., and Bachman, S. B., eds., **38**, 1-16, 1984.

Minster, J. B., T. H. Jordan, P. Molnar, and E. Haines, Numerical modelling of instantaneous plate tectonics, *Geophys. J. R. Astron. Soc.*, **36**, 541-576, 1974.

Ness G., S. Levi, and R. Couch, Marine magnetic anomaly timescales for the Cenozoic and late Cretaceous: a precis, critique, and synthesis, *Rev. Geophys.*, **18**, 753-770, 1980.

Penrose, R., A generalized inverse for matrices, *Proc. Cambridge Philos. Soc.*, **51**, 406-415, 1955.

Shapiro, I. I., Use of Space Techniques for Geodesy, in *Proceedings of the International School of Physics--Enrico Fermi--Earthquakes: Observations, Theory, and Interpretation*, H. Kanamori, ed., pp. 530-568, North-Holland, Amsterdam, 1983.

Sieh, K. E., and R. H. Jahns, Holocene activity of the San Andreas fault at Wallace Creek, California, *Geol. Soc. Amer. Bull.*, **95**, 883-896, 1984.

Smith, D. E., R. Kolenkiewicz, P. J. Dunn, and M. H. Torrence, The measurement of fault motion by satellite laser ranging, *Tectonophysics*, **52**, 59-67, 1979.

Smith, D. E., D. C. Christodoulidis, R. Kolenkiewicz, P. J. Dunn, S. M. Klosko, M. H. Torrence, S. Fricke, and S. Blackwell, A global geodetic reference frame from Lageos ranging (SL5.1AP), *J. Geophys. Res.*, **90**, 9221-9234, 1985.

Talwani, M., C. C. Windisch, and M. G. Langseth, Jr., Reykjanes Ridge Crest: a detailed geophysical study, *J. Geophys. Res.*, **76**, 473-517, 1971.

Tapley, B. D. , B. E. Schutz, and R. J. Eanes, Station coordinates, baselines and earth rotation from Lageos ranging: 1976-1984, *J. Geophys. Res.*, **90**, 9235-9249, 1985.

Vogt, P. R., Plate motions over the last 10-20 Ma and the problem of "present" motions, in *Decade of North American Geology: The Western Atlantic Region*, Geological Society of America, Tucholke, B.E., and P. R. Vogt, eds., in press, 1985.

TABLE 1. SL6 ANNUAL SOLUTION STATION SUMMARY

					NORMAL POINT DISTRIBUTION					
SITE LOCATION	STATION	LAT(N)	LON(E)	HEIGHT(M)	78	79	80	81	82	83
KOOTWIJK, HOLLAND	7833	51.992	5.810	86	-	-	158	-	217	272
WETTZELL, GERMANY	7834	48.954	12.878	654	154	145	112	132	779	545
GRASSE, FRANCE	7835	43.563	6.921	1315	-	76	317	-	540	-
AREQUIPA, PERU	7907	-16.361	-71.493	2485	-	880	1515	1372	5261	5997
MT HOPKINS, ARIZ	7921	31.513	-110.878	2345	1868	-	-	-	55	-
NATAL, BRAZIL	7929	-5.888	-35.165	32	303	-	88	231	-	-
ORROPAL, AUSTRALIA	7943	-35.443	148.955	941	1729	1625	3245	884	120	-
QUINCY 1, CALIF	97051	39.784	-120.940	1052	-	103	-	1283	-	-
OTAY MT, CALIF	97062	32.426	-116.841	981	-	368	-	302	-	123
GSFC, MARYLAND	97063	38.832	-76.828	12	520	-	-	848	-	-
BEAR LAKE, UTAH	97082	41.742	-111.421	1955	-	286	-	298	-	-
FT DAVIS, TEXAS	97086	30.508	-104.016	1954	-	537	1094	-	-	894
YARAGADEE, AUSTRALIA	97090	-28.883	115.347	234	-	112	6389	6594	5219	1919
HAYSTACK, MASS	97091	42.431	-71.488	84	168	1035	1992	-	-	-
KWA ATOLL, MARSHALL IS	97096	-14.243	-170.725	42	-	171	671	-	-	-
GSFC 102, MARYLAND	97102	38.833	-76.828	10	-	109	521	2543	675	290
QUINCY 2, CALIF	97109	39.786	-120.945	1099	-	-	-	165	1589	3193
MONUMENT PEAK, CALIF	97110	32.717	-116.423	1831	-	-	-	915	2357	1138
PLATTEVILLE, COLO	97112	39.993	-104.726	1494	-	-	-	1319	2383	790
OWENS VALLEY, CALIF	97114	37.047	-118.294	1170	-	1194	1724	37	286	175
GOLDSTONE, CALIF	97115	35.067	-116.792	1035	-	927	1994	772	-	-
HALEAKALA, HAWAII	97120	20.581	-156.256	3060	-	-	-	2543	163	-
VERNAL, UTAH	97892	40.137	-109.571	1582	-	-	-	362	206	-

STATION	EPOCHS		MOTION		MAJOR	MINOR	AZ
			N(cm)	E(cm)	cm	cm	deg
7833	3	5	-15.63	19.46	41.56	28.62	93.81
7833	5	6	32.97	-26.82	42.24	26.54	94.42
7834	1	2	-46.76	-6.81	62.25	53.91	133.40
7834	2	3	-2.23	-9.12	52.67	50.22	12.07
7834	3	4	22.18	13.62	47.86	40.23	55.95
7834	4	5	-23.53	12.79	37.74	29.59	63.46
7834	5	6	1.77	14.25	25.52	19.41	94.23
7835	2	3	10.23	58.28	44.63	39.94	89.07
7835	3	5	31.94	-1.56	28.16	23.46	106.56
7907	2	3	-0.98	9.36	22.38	18.33	2.48
7907	3	4	12.69	-6.50	23.80	14.28	15.40
7907	4	5	-2.12	5.18	22.77	11.58	17.37
7907	5	6	3.40	17.13	17.20	9.47	13.40
7921	1	5	73.22	-31.67	62.37	35.52	132.95
7929	1	3	-43.14	-61.18	45.83	39.32	28.71
7929	3	4	-16.23	-22.12	41.77	34.19	25.48
7943	1	2	1.89	3.86	32.02	26.62	110.71
7943	2	3	8.32	0.72	28.81	16.29	111.55
7943	3	4	12.48	-8.14	19.92	13.78	123.12
7943	4	5	-12.37	19.46	29.21	24.83	120.92
97081	2	4	-2.10	-6.78	36.47	31.78	121.40
97082	2	4	2.35	-7.64	32.94	24.68	109.72
97082	4	6	5.30	-7.47	28.30	26.40	132.49
97083	1	4	11.70	2.74	24.58	17.82	18.08
97086	2	4	4.95	9.11	36.27	32.11	120.78
97086	2	3	-5.46	9.33	20.32	17.37	127.79
97086	3	6	-0.52	-9.47	18.86	12.39	157.49
97090	2	3	6.9.	7.04	39.56	31.73	87.67
97090	3	4	4.34	0.11	18.09	13.20	96.46
97090	4	5	-2.67	14.32	17.39	11.55	93.89
97090	5	6	16.73	4.92	16.72	12.23	92.91
97091	1	2	17.89	28.22	33.58	26.74	77.83
97091	2	3	-4.83	-4.23	14.27	13.92	150.14
97096	2	3	16.27	26.35	45.[illegible]	26.26	128.90
97102	2	3	29.87	-8.86	23.77	20.35	122.06
97102	3	4	-1.10	-17.21	19.83	17.74	29.31
97102	4	5	-8.85	11.87	18.78	16.40	22.19
97102	5	6	-5.71	3.94	19.83	17.66	172.73
97109	4	5	1.99	5.72	23.58	19.23	18.81
97109	5	6	-8.01	8.88	10.86	8.[illegible]	148.[illegible]
97110	4	5	3.34	-7.18	18.67	10.[illegible]	151.24
97110	5	6	-6.36	6.42	13.27	8.87	167.31
97112	4	5	-2.42	1.05	13.23	11.32	164.76
97112	5	6	-12.32	1.22	13.22	10.35	150.24
97114	2	3	-6.18	5.62	21.32	16.30	134.86
97114	3	4	9.02	-6.32	21.32	13.66	147.08
97114	4	5	-11.33	8.66	23.62	21.39	162.72
97114	5	6	-11.42	-0.03	23.21	20.57	7.76
97115	2	3	-7.94	7.23	21.31	16.47	139.77
97115	3	4	-3.88	-4.51	17.70	17.30	139.71
97120	4	5	-3.89	16.31	29.23	23.[illegible]	125.13
97892	4	5	-4.37	4.79	23.72	23.31	151.24

TABLE 2. SLR VECTOR DATA

Epochs= Initial and final epoch corresponding to vector motion. Motions local geodetic north and east components of apparent station position motion vector. Major,Minor,Azm Semi-major,and minor axis and azimuth in degrees clockwise from north of the tangential error ellipse associated with the motion vector.

Epoch-Subset Results

Epochs	#Data	$\tilde{\gamma}$	σ_{γ}	$\hat{s}^2$	$\hat{\sigma}_{\gamma}^2$
1,2	3	-3.470	0.450	0.009	22.540
2,3	11	0.439	1.090	0.392	3.028
3,4	8	1.308	0.673	0.348	1.303
4,5	11	1.248	0.372	0.179	0.770
5,6	9	0.514	0.501	0.345	0.726
1,2,3	15	-0.226	0.816	0.368	1.810
2,3,4	22	0.905	0.423	0.315	0.568
3,4,5	21	1.275	0.270	0.279	0.260
4,5,6	21	0.969	0.258	0.277	0.241
1,2,3,4	27	0.587	0.389	0.363	0.418
2,3,4,5	35	1.184	0.232	0.287	0.187
3,4,5,6	32	1.120	0.194	0.341	0.110
1,2,3,4,5	41	0.963	0.218	0.327	0.145
2,3,4,5,6	46	1.061	0.171	0.335	0.087
1,2,3,4,5,6	52	0.947	0.160	0.355	0.072

Table 3. Results from estimation of rate-scaling parameter based on epoch-subsets of the data. Epoch 1 = 1978, epoch 6 = 1983, etc; #Data = number of relative motion vectors observed during interval; the other quantities are defined in the text; all stations used for each estimation.

Table 4. Comparison of Talwani *et al.* (1971) and Ness *et al.* (1980) marine magnetic anomaly timescales, with corresponding estimate of rate-scaling parameter.

Anomaly	Talwani(m.y.)	Ness(m.y.)	γ (T/N)
1	0.00	0.00	1.000
	0.69	0.72	0.958
1'	0.89	0.91	0.978
	0.95	0.97	0.979
2	1.71	1.66	1.030
	1.86	1.87	0.995
2'	2.43	2.47	0.934
	2.84	2.91	0.976
	2.94	2.95	0.997
	3.04	3.07	0.992
	3.10	3.17	0.978
	3.32	3.40	0.976
3	3.78	3.86	0.979
	3.88	3.98	0.975
	4.01	4.12	0.973
	4.17	4.26	0.979
	4.31	4.41	0.977
	4.41	4.49	0.982
	4.48	4.59	0.976
	4.66	4.79	0.973

Figure Captions

Figure 1. Nominal SLR station positions used to estimate rate-scaling parameter. Station locations corresponding to site number are listed in Table 1.

Figure 2. Data, consisting of apparent tangential vector motions of network sites positions between successive epochs with associated tangential one-sigma (unscaled) error ellipse, used to estimate rate-scaling parameter. Also listed in Table 2.

Figure 3. Estimate of rate-scaling parameter as a function of total number of motion vectors utilized in epoch-subset trials. Dashed line is the RM2 reference estimate. Error bars are one-sigma (scaled by sampling variance). Values listed in Table 3.

Figure 4. Estimate of rate-scaling parameter as a function of the temporal averaging interval. RM2 is the reference estimate with 1 m.y. error bars. One- and five-year SLR-derived estimates have errors as in Figure 3. Values listed in Table 3. NLC-80 are estimates derived from the comparison of the Talwani *et al.* (1971) marine magnetic anomaly timescale, upon which the RM2 rates are based, and Ness *et al.* (1980) timescale, as listed in Table 4. Variability of NLC-80 about RM2 is well within the five-year SLR-derived one-sigma level of confidence.

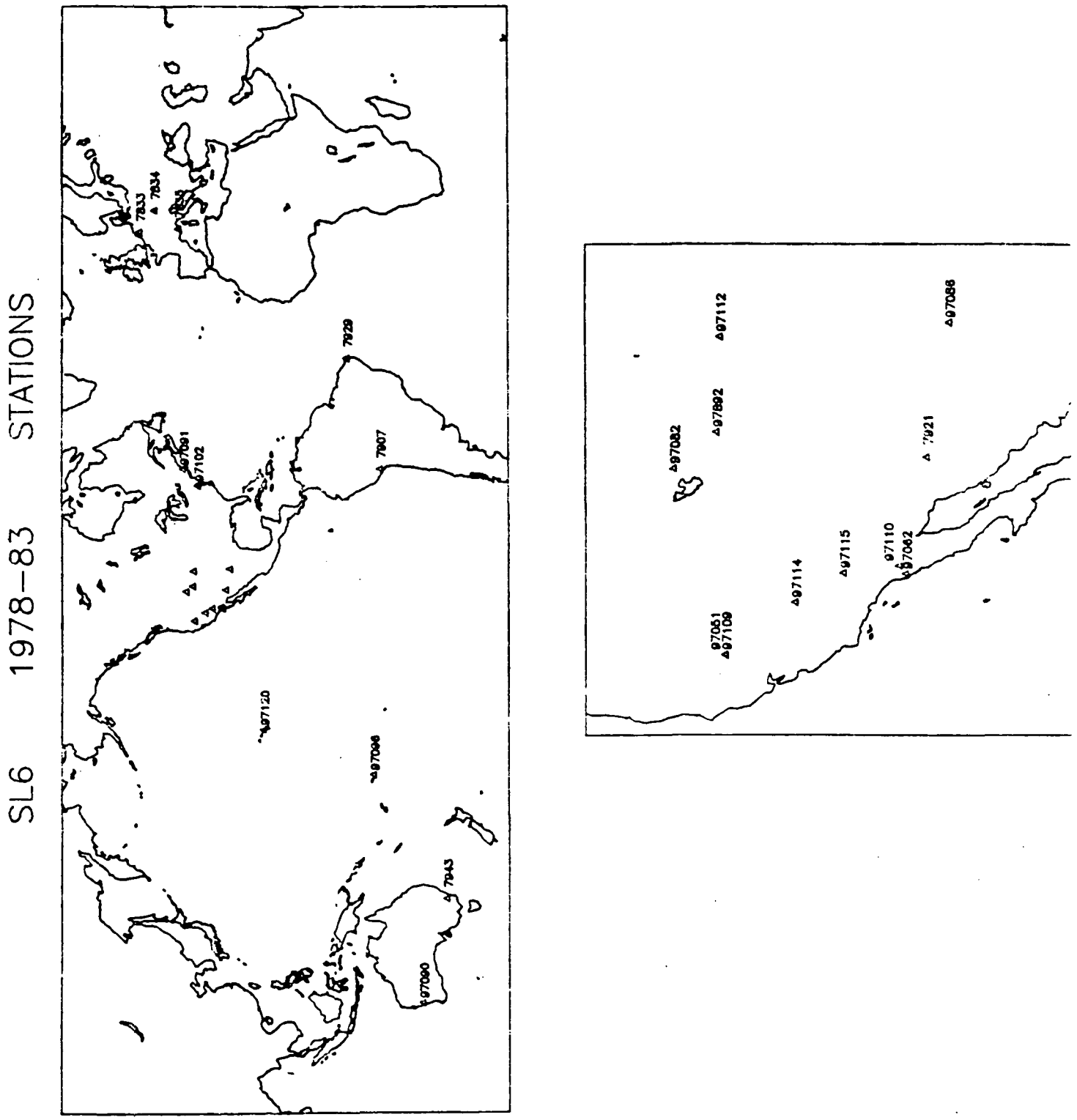

Figure 1

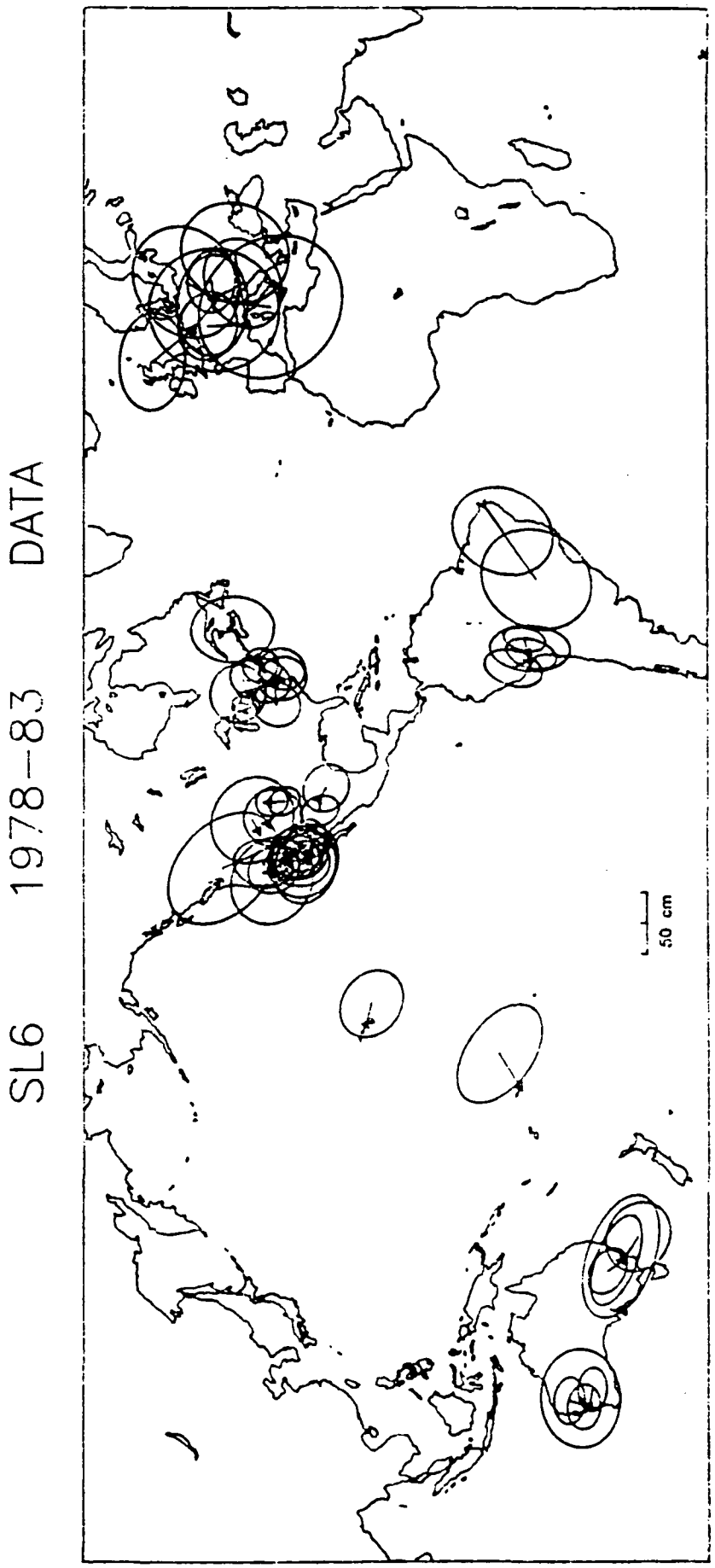

Figure 2

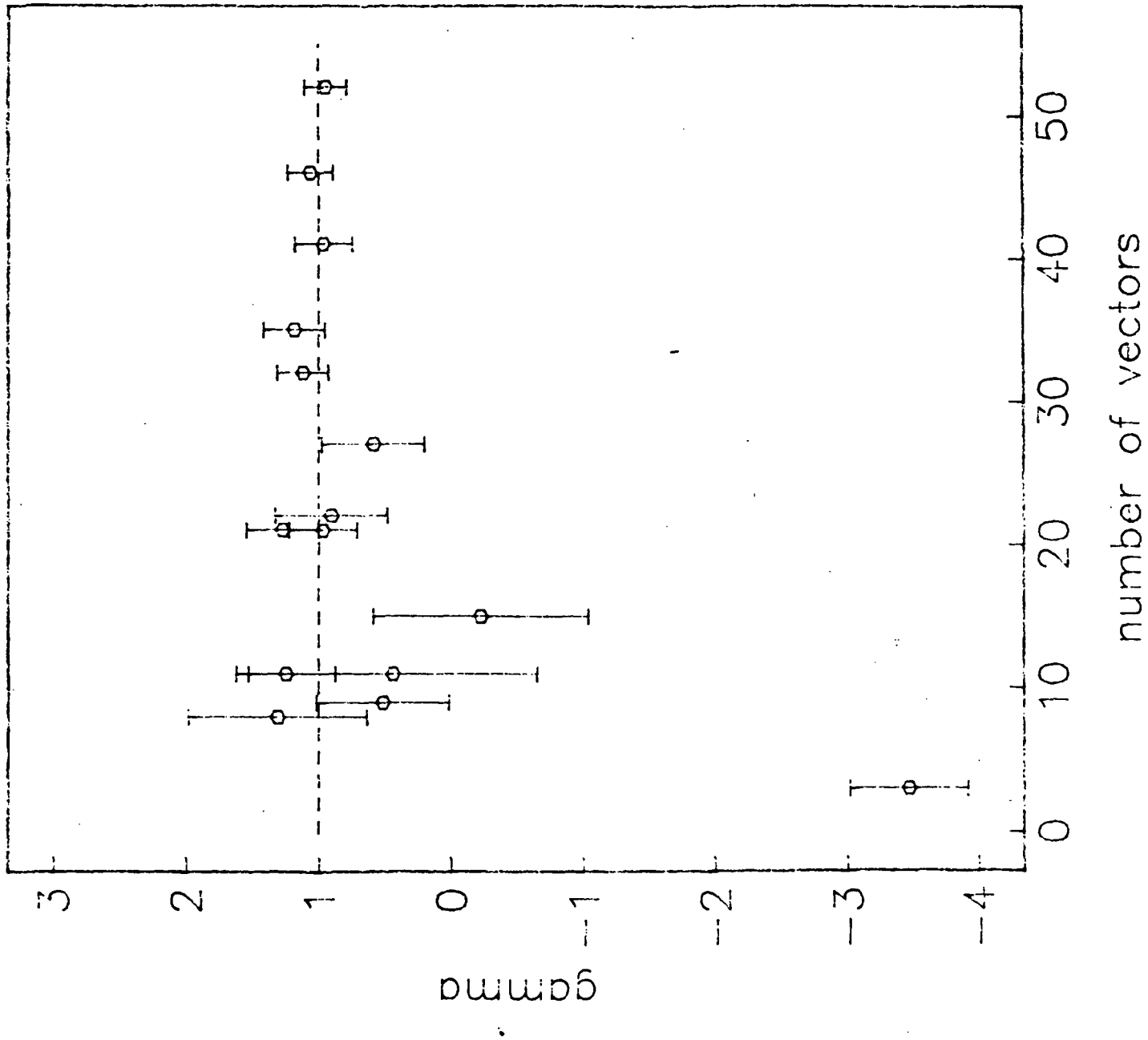

Figure 3

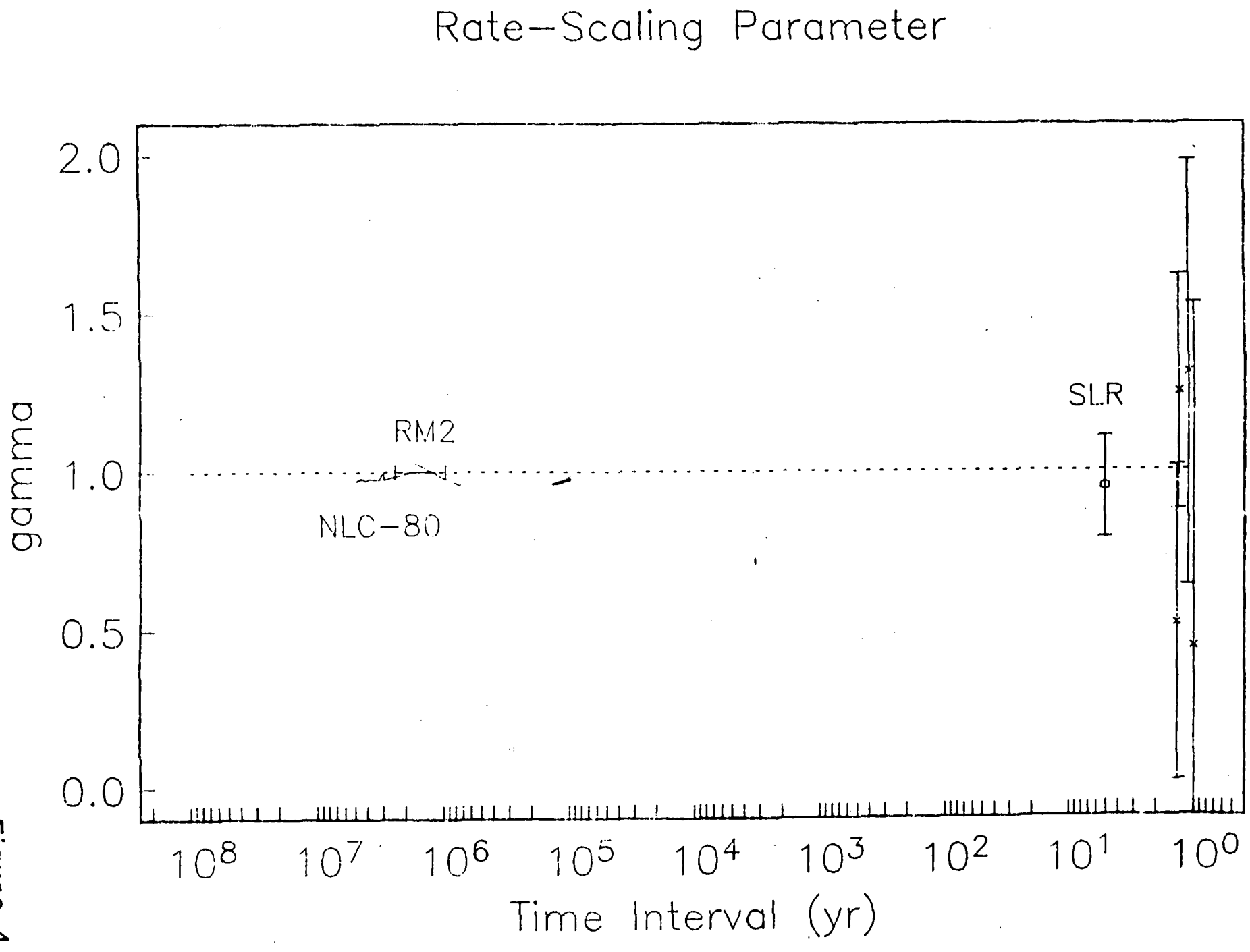
Rate–Scaling Parameter
2.0
1.5
1.0
0.5
0.0
gamma
RM2
NLC–80
SLR
10^8 10^7 10^6 10^5 10^4 10^3 10^2 10^1 10^0
Time Interval (yr)

Figure 4